Abstract: This doctoral thesis is dedicated to the study of magnetization dynamics in ferromagnetic semiconductor (Ga,Mn)As using magneto-optical (MO) spectroscopy methods. The character of the magnetization dynamics after the impact of the laser pulse was investigated under different experimental conditions in an extensive set of optimized (Ga,Mn)As samples with Mn doping ranging from 1.5% to 14%. The thorough analysis of the measured MO signal enabled us to develop a new method that can be used to determine the laser pulse-induced real-space magnetization trajectory without any numerical modelling. Moreover, the investigation of the measured MO signals allowed us to determine the basic micromagnetic properties of (Ga,Mn)As, such as the magnetic anisotropy, the Gilbert damping or the spin stiffness. In addition to this, we found out that the light-induced magnetization precession can be caused by three distinct mechanisms - the sample heating due to the energy transfer from the laser pulses, the angular momentum transfer from the circularly polarized photons, and the influence of the non-equilibrium hole polarization induced by the relativistic spin-orbit interaction. The first of these mechanisms is rather well known but the two remaining ones, which are the optical analogues of the spin-transfer torque and the spin-orbit torque, were not reported in the literature so far.

PREFACE

Over the past few years, there has been a considerable interest and progress in investigation and understanding of the spin-related phenomena. The majority of the research was focused on the spin states and dynamics in magnetic metals and it led to a development of devices with improved or completely new functionalities, which are typically based on the giant magnetoresistance (GMR) or similar effects. These effects are used in devices such as hard disc read heads, non-volatile memory chips or in magnetometers. However, the discovery of the magnetic order in semiconductors has opened a new perspective for the spin-based electronics (spintronics). For example, the incorporation of Mn ions into the conventional GaAs semiconductor showed unprecedented features of magnetism in (Ga,Mn)As, where the Mn atoms act as localized magnetic moments on one hand, and introduce free holes into the system on the other hand. The high concentrations of holes give rise to a strong, so called carrier-mediated, ferromagnetic order between the Mn spins, enabling the direct control of magnetism by external means (optically, by electrical field, etc.). A part of (Ga,Mn)As research is also devoted to fast manipulation of the magnetic order by ultrashort laser pulses as it is a challenging topic with potential impact on the time scale of information manipulation and processing.

This thesis is dedicated to the study of magnetization dynamics after the impact of the ultrashort (femtosecond) laser pulse on (Ga,Mn)As by means of the time-resolved magneto-optical (MO) spectroscopy. The analysis of the MO signals enabled investigation of the basic micromagnetic material properties, such as the magnetic anisotropy, Gilbert damping parameter, or the spin stiffness. Moreover, the MO spectroscopy served us as a very useful tool for revealing some of the predicted, yet experimentally unobserved physical phenomena. The time-integrated MO spectroscopy was utilized in order to investigate the electronic structure, thus the origin of the magnetic interactions in (Ga,Mn)As. This thesis can be considered as experimental but it is also supplemented with some simple calculations that were beneficial for the interpretation of the experimental results. The overwhelming part of the experiments was performed in the laser laboratory of the Department of Quantum Optics and Optoelectronics at Charles University in Prague and the smaller part in the Department of Physics at University at Buffalo.

I have taken advantage of the possibility to write my thesis in the form of commented set of published or submitted articles. I have chosen this form because the output of my work during the past four years is very clearly and systematically documented in the already written articles, which give the reader a comprehensive insight on my work. Hence, the thesis is divided into two parts – the first part gives a general overview of the theoretical and experimental findings in the magneto-optical research of (Ga,Mn)As. The main emphasis is put on the description of the laser-induced magnetization dynamics, its origin and its significance in characterizing the basic micromagnetic properties of (Ga,Mn)As. This overview was written with respect to the results presented in the second part, given by a set of articles in the Appendices 1 – 8.

Contents

1. Introduction

The current electronics based on the carrier charge transport for information storage and processing is reaching its limits due to the ongoing miniaturization of transistors. According to the Moore's law, the progress of complementary metal-oxide-semiconductor (CMOS) technology has increased rapidly, i.e. the number of transistor that can be integrated on one chip has been doubled every two years. With the advanced laser photolithography the gate size has shrank to 20 nm and the transistor density has already reached over ~ 10^6/mm^2 with the switching speeds up to 10 GHz [1]. The future semiconductor logic device with the suggested 10 nm gate width will, however, face the essential energy problems, since the projected gate-switching energy (the energy needed to switch between two logical states "0" and "1") in 2020 for low-standby-power and fast CMOS transistors is three orders of magnitude larger than the theoretical minimum [1, 2]. Thus the CMOS technology is approaching its "dead end" not only because of the unsatisfying energy management but also for the physical limitations on the transistor gates. In order to fulfill the increasing demands on more powerful technologies, we need to create a new class of energy saving (non-volatile) and high speed switching (THz) devices that would exploit new physical approaches. Spintronics provides a possibility of utilizing the carrier spin, as an addition or alternative to its charge, for the information transport and storage which could not only improve the performance but also add new functionalities to the existing devices [1, 3]. The electrical and spin properties are, however, characterized by different properties. The electrical properties are given by carrier mobility, electrical conductivity or electrical current whereas the spin properties are described by magnetization, magnetic resonant frequencies and spin relaxation rates. The tools that control the electron charge and spin are also different – while the electronic devices are manipulated by the applied voltages, the spin state is predominantly controlled by magnetic fields. This diversity drives the need for a search of new materials in which both approaches could be merged. Current spintronics is based mainly on ferromagnetic (FM) metals, exploited for example in commercially successful spin valves which are used in hard disc read heads or magnetic random memories (MRAM). Spin valves are based on the giant/tunneling magnetoresistance principles, where the resistance magnitude is changes by the applied magnetic field. The possibility of changing the physical properties by electrical field is a feature of semiconductors. The biggest obstacle in smooth integration of magnetic materials into information processing circuits is the lack of efficient control of their magnetization. As it was previously mentioned, this is vastly achieved with external magnetic fields which - in contrast to electric fields - cannot be applied locally. The demonstration of ferromagnetism in diluted magnetic semiconductors (DMS) raised hopes for applications based on single element combining the information storage capabilities of magnetic metals with the logic functionalities of semiconductors.

DMS are alloys consisting of a non-magnetic semiconductor doped with small percentage of magnetic impurities (most commonly Mn atoms). It was shown that such a small doping with magnetic ions (~ several percent) will not deteriorate the optical or

transport properties of the host and will introduce large magnetic and magneto-optical effects [4, 5]. The extensive study of DMS and their heterostructures has started with II-IV semiconductors, mostly CdTe and ZnSe [6, 7], but it was soon discovered that the FM order is present only at very low temperatures (below 2 K [6]), so the research has subsequently moved to III-V compounds. Nowadays, the most thoroughly investigated DMS is (Ga,Mn)As, with the highest Curie temperature (T_C) among all the DMS, $T_C \sim 190$ K [8, 9]. In (Ga,Mn)As the FM order is established by an exchange interaction between the charge carriers (holes) and the localized Mn spins (see Chap. 2) [6]. The carrier concentration is relatively low, of the order of 10^{20} to 10^{21} cm^{-3} (depending on Mn doping), as opposed to 10^{23} cm^{-3} in metals [10], so it is possible to control the amount of carriers by external electric fields, which not only influences the electronic properties but also the stability of ferromagnetic phase and other magnetic properties [11]. Despite the fact that T_C of (Ga,Mn)As is still far below the room temperature and its further increase is questionable [10, 12], it has already played a crucial role in exploring new physics, ideas and concepts in spintronics that has not been accessible in metals. In the following paragraph we summarize some of the most interesting phenomena that were observed in (Ga,Mn)As – some of them serve "only" as a proof of spintronic concepts but some have stimulated a discovery of related phenomena in conventional metals magnets, which are highly relevant for current spintronic applications [4, 10].

As already mentioned, the tunneling magnetoresistance (TMR) is one of the building blocks of spintronics, which is currently commercially utilized for the information readout in FM metals. The well-established growth of heterostrustructures and microfabrication techniques in semiconductors enabled fabrication of the high quality tunnel junctions which showed large TMR in III-V compounds as well [13, 14]. In particular, an intrinsic TMR effect with magnetoresistance up to 100% was observed in a device containing two (Ga,Mn)As electrodes separated by ZnSe tunneling barrier [14]. Besides the conventional two FM electrode devices (also called the Mott devices), (Ga,Mn)As served as a key material for observing the tunneling anisotropic magnetoresistance (TAMR) which comprise only one FM electrode. This phenomenon originates from the spin-orbit coupling (SOC) which causes that the conductivity depends on the orientation of the magnetization relative to the crystal axis or the current direction, so there is no need for the reference electrode. Devices based on the SOC are generally called the Dirac devices as the SOC was elucidated in Dirac equation [15]. The TAMR was primarily observed in (Ga,Mn)As [16] and subsequently detected in conventional metals [17]. Another type of magnetoresistance – the Coulomb blockade anisotropic magnetoresistance (CBAMR) – was observed in (Ga,Mn)As single electron transistor (SET) [18]. In this effect the electron can tunnel through a tunneling barrier due to the Coulomb blockade oscillations, which can show both positive and negative spin-valve-like characteristics depending on the SET gate voltage. This new type of magnetoresistance should be generic to SETs fabricated in FM systems with large SOC and we note that for, e.g. FePt FM metal this effect was predicted to be observable even at room temperature [18]. Such effect could be utilized in the next generation devices, analogous to the field effect transistors (FET), where the spin transport and the magnetoresistance magnitude would be controlled by a voltage applied to the gate. Another step towards a fundamentally new information processing paradigm was again realized in (Ga,Mn)As – a monolithic read-write

device. In this single device, the information is written as a magnetic state ("0" and "1" are represented by two *perpendicular* orientations of magnetization) by current-induced switching and readout of the state is done by means of the TAMR effect [19]. The current densities that are needed to switch the magnetization from one state to another are on the order of ~ 10^5 Acm^{-2}, which is 1 to 2 orders of magnitude lower than the densities needed in metallic memory elements [19]. Such device has a lot of technological advantages as it allows for manufacturing the integrated circuits consisting of identical multifunctional elements, which can be easily and cheaply produced. We finish the list of intriguing phenomena observed in (Ga,Mn)As by mentioning the reversible control of magnetization orientation using the spin-orbit magnetic field, i.e., by so called spin-orbit torque (SOT). In contrary to the spin transfer torque (STT), where a spin polarized current induces a torque on magnetization via the angular momentum transfer [20, 21, 22], in SOT the equilibrium orientation of magnetization is changed by an *unpolarized* current due to the relativistic spin-orbit coupling [23, 24]. A device based on the SOT principle was constructed by Chernyshov et *al.* [23] and performs a non-volatile memory cell, with two states (2 bits) encoded in the magnetization direction which is controlled by the unpolarized current passing through the device in one crystallographic direction. The authors suggest that the functionality of the device could be increased into 4 bits, if the current is injected in two orthogonal directions.

Despite the fact that (Ga,Mn)As is thoroughly investigated material, as could be seen from the previous paragraph, its properties are still not understood completely. For example, there is an ongoing debate about the character of its electronic band structure, mainly the position of the Fermi level for Mn doping exceeding 1 % [25, 26, 27]. There is also a large scatter in the micromagnetic parameters magnitude that seemed to be lacking any monotonous dependence on Mn doping. This thesis is dedicated to the study of some of the basic (Ga,Mn)As properties (electronic band structure) and parameters (anisotropy constants, spin stiffness or Gilbert damping coefficient), employing both, the time-integrated and time-resolved magneto-optical methods. Moreover, we report on two newly discovered physical phenomena, concretely on the optical counterparts of STT and SOT.

2. Ferromagnetic semiconductor (Ga,Mn)As

The significance of (Ga,Mn)As can be seen from several aspects. i) The incorporation of Mn atoms causes only a small perturbation of the GaAs host, which is the mainstream semiconductor used in high-mobility transistors, lasers and other electronic devices. Incorporating the FM order into this highly used semiconductor is thus very attractive. ii) The magnetism in (Ga,Mn)As is mediated by the charge carriers (as will be discussed later in more detail), so the magnetic properties can be controlled, in addition to magnetic, also by the electric field. iii) Nowadays, the growth techniques and the subsequent postgrowth treatment are well managed and the structures on the nanometer scale can be fabricated by the advanced microfabrication methods. All these attributes, together with a potential for future applications, motivate the extensive research of (Ga,Mn)As. This chapter is devoted to a brief overview of its most essential properties, focusing especially on the magnetic ones.

2.1 Magnetic order

When a magnetic Mn atom is incorporated into GaAs, it occupies the cation (Ga) sublattice (Mn_{Ga}) in the zinc-blend host structure [25, 28]. As can be seen from nominal atomic composition of each element: [Ar]$3d^{10}4s^2p^1$ for Ga, [Ar]$3d^5 4s^2$ for Mn, and [Ar]$3d^{10}4s^2p^3$ for As, Mn_{Ga} not only provides a localized spin $S = 5/2$ due to five 3*d* electrons, but also acts as an acceptor, because of the missing 4*p* valence electron. The concentration of provided holes and Mn moments is crucial for establishing the FM order in the system. One could assume that the concentration of Mn ions corresponds to the same concentration of holes and Mn moments. This is, however, not true in the real systems, since Mn atoms can also occupy the less energetically stable interstitial (Mn_I) positions (see Fig. 1), acting as double donors and compensating the concentration of holes [28]. Moreover, the Mn_I also couples antiferromagnetically to Mn_{Ga}, reducing the overall magnetic moment [28]. The number of Mn atoms that *effectively* contribute to the ferromagnetic order can be defined as: $Mn_{eff} = Mn_{sub} - Mn_I$, where Mn_{sub} and Mn_I stand for substitutional and interstitial Mn atoms, respectively [26].

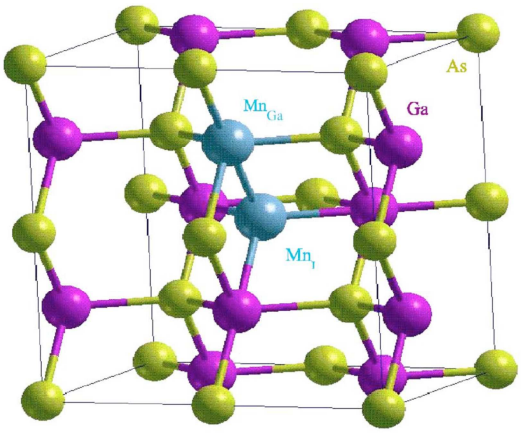

Fig. 1: (Ga,Mn)As unit cell. The most energetically favorable position of Mn atom in the GaAs host cell is in the position of Ga (Mn_{Ga}). The less common interstitial position is depicted as Mn_I. [27]

The origin of ferromagnetism in (Ga,Mn)As was studied both, theoretically and experimentally and the proposed explanation can be found in Refs. 25, 28, 29, 30, here, only the basic picture is given. In this elementary framework – which is still a matter of controversy [25, 27, 31] – the ferromagnetic coupling between Mn spins is mediated by the free carriers (holes). The strong *p-d* hybridization between holes and localized Mn *d* electrons results into their antiferromagnetic (AF) interaction, which can be described by the exchange parameter J_{pd}. The spin polarized holes transfer their AF coupling with Mn spins further into the lattice, causing the long-range overall FM order between the localized Mn spins [28]. Experimentally, the FM in $Ga_{1-x}Mn_xAs$ is observed when the Mn doping reaches ~ 1% (x = 1% corresponds to Mn concentration of $2.2\text{x}10^{20}$ cm^{-3} [27]), which is well above the equilibrium solubility limit in GaAs and therefore the non-equilibrium molecular beam epitaxy (MBE) technique is used for the growth. The overall strength of the magnetic order is characterized by the Curie temperature T_C that is, in the simplified approach, directly proportional to the effective Mn and hole concentrations, x_{eff} and p, respectively [29, 30]. In addition, T_C was found to be the most simple and reliable parameter for characterizing the quality of (Ga,Mn)As samples. The highest attainable T_C leads simultaneously to layers with maximized uniformity and minimized compensation by unintentional impurities and defects [8, 32]. In order to produce high quality samples with the lowest concentration of defects, the samples have to be grown and subsequently annealed under optimized conditions, which vary for each nominal Mn doping x. For detailed description of the growth and annealing conditions see Němec et *al*. [33] in Appendix 8.

2.2 Electronic band structure

In the first approximation, (Ga,Mn)As has very similar band structure to GaAs, consisting of a conduction and valence band, where the later one is split into three sub-bands (heavy, light and split-off bands), due to the spin-orbit interaction [34, 35]. However, the *exact* electronic structure of this material is still widely discussed, lacking an unambiguous explanation mainly for higher concentrations of Mn ions [31, 36]. The picture is clear and well accepted only for a single Mn impurity in GaAs host structure, where it forms a separate impurity level which is detached (~ 0.1 eV) from the top of the valence band (VB). This impurity level is formed due to three main contributions [36]: i) long-range acceptor hydrogenic-like potential, ii) short-range central cell potential, which is specific for a given impurity and iii) spin-dependent hybridization of Mn *d*-levels with As *p*-levels. This single impurity model persists only for low Mn concentrations ($x \ll 1\%$), where the free carrier density is below the metal-to-insulator transition [31, 36]. In this scenario, the Fermi level resides in a narrow impurity band (IB). For concentrations $x > 1.5\%$, where the conductivity increases by several orders of magnitude [33, 36] and where the material becomes a degenerate semiconductor (i.e. with a metallic-like conductivity), two physical scenarios exist, named the *valence* and *impurity* band, respectively [26, 31, 33, 36, 37, 38, 39, 40]. In the VB model, the detached impurity band broadens with increasing Mn doping, and for sufficiently screened hydrogenic-like potential, it merges into the valance band. The states at the Fermi energy (E_F) retain the *p*-orbital character of the host semiconductor [28, 32, 36]. On

the other hand, the IB model predicts the persistence of the impurity band (as well as E_F) within the band gap also for the high-doped (Ga,Mn)As layers with metallic-like conduction [26, 37, 38, 39, 40]. While the VB model is built on the tight-binding approximation Hamiltonian, treated using the Anderson model (for magnetic impurities) and the coherent potential approximation (for disorder) [36], the IB model lacks suitable theoretical background and its whole framework is based only on the experimental results that contradict the predictions of the VB model.

For further discussion about the electronic structure of (Ga,Mn)As see Chap. 3, where the character of bands (and the related origin of FM order) is reviewed in the light of static magneto-optical measurements (magnetic circular dichroism in particular).

2.3 Magnetic anisotropy

For typical Mn doping levels 1% - 10% in (Ga,Mn)As, the magnetocrystalline anisotropy dominates over the shape anisotropy, that is prevailing in conventional ferromagnets [41]. Magnetocrystalline anisotropy describes the ferromagnet energy dependence on the magnetization orientation with respect to the crystallographic axes, and is originating mainly from a strong spin-orbit coupling of holes in the valence band [35]. The overall magnetic anisotropy (MA) is given by a sum of different anisotropy fields and the external magnetic field. In (Ga,Mn)As, the MA is dominated by the cubic and uniaxial anisotropies (in a case when no external magnetic field is applied) [41]. The cubic anisotropy reflects the zinc-blend symmetry of the GaAs host in which [100], [010] and [001] crystallographic directions are equivalent. However, in (Ga,Mn)As the symmetry between the in-plane and out-out-of-plane directions is distorted, due to additional compressive strain induced by the substrate (in the case of GaAs substrate). The cubic anisotropy is thus replaced by the biaxial (more often called in-plane "cubic", K_c) and the out-of-plane (K_{out}) anisotropies [28, 41]. The uniaxial in-plane anisotropy (K_u) is not associated with any measurable strain in the epilayer and is likely of the extrinsic origin (caused by the low-temperature MBE growth) [41, 42], favoring the [-110] crystallographic direction. MA is given by a total free energy functional F, which can be written as [41, 43]:

$$F = M\left[\begin{array}{l} K_c \sin^2\theta\left(\frac{1}{4}\sin^2 2\varphi \sin^2\theta + \cos^2\theta\right) - K_{out}\cos^2\theta - \frac{K_u}{2}\sin^2\theta(1-\sin 2\varphi) - \\ - H_{ext}\left[\cos\theta\cos\theta_H + \sin\theta\sin\theta_H\cos(\varphi-\varphi_H)\right] \end{array}\right], \quad (1)$$

where the angles φ (φ_H) and θ (θ_H) describe the orientation of magnetization (external magnetic field H_{ext}) from the [100] and [001] crystallographic axes, respectively. The minimum of the free energy functional determines the equilibrium position of magnetization, usually denoted as the *easy axis* (EA). It is important to remark, that the EA position is very sensitive to the "inherent" material properties, such as the hole concentration (p) and the magnetic moment magnitude (M) and also to the "external" conditions, such as temperature (T) or strain, as every magnetic anisotropy component K_i is a function of p, M, T and strain [41, 44, 45]. We note that (Ga,Mn)As is a highly disordered material, mainly because of the

non-equilibrium low temperature growth by the MBE technique, which causes a high number of different defects (see Chap. 2.1) [46]. This influences the number of uncompensated holes (p) and also the magnetic moment magnitude. In order to increase the hole concentration and the overall magnetic quality, the samples are annealed and/or etched after the growth [33, 46].

The magnitude of the magnetic anisotropies can be determined by at least three independent methods, e.g. by the ferromagnetic resonance (FMR) [47, 48], by the superconducting quantum interference device (SQUID) [49] or by the time-resolved magneto-optical spectroscopy. As part of this thesis is devoted to the determination of the magnetic anisotropy constants from the time-dependent magneto-optical signal, the detailed description of this method can be found in Chap. 6, or see Němec et *al*. [33] in Appendix 8.

2.4 (Ga,Mn)As samples used in this thesis

All the experimental results presented in this thesis (see Appendices 1 – 8) were obtained on the set of $Ga_{1-x}Mn_xAs$ samples, which are summarized in Table 1. The samples were grown at the Institute of Physics of the Academy of Sciences in Prague by the non-equilibrium MBE method. All the samples were of very high-quality, with relatively high Mn doping, spanning the range from x = 1.5% to 14%. The details about the growth and post-growth treatment can be found in Ref. 33 (see Appendix 8). All samples are in-plane magnets in which the biaxial anisotropy is competing with the uniaxial. In the lowest Mn doping (x = 1.5%), the biaxial anisotropy dominates and the EA lies in the [100] or [010] crystallographic direction. With increasing Mn concentration, the uniaxial anisotropy starts being comparable with the biaxial, shifting the EA towards the [-110] direction. The uniaxial anisotropy dominates for x > 9% and the EA is aligned with [-110] crystallographic direction. The samples show increasing magnetic moment M_S, T_C and p with increasing Mn concentration [33].

sample	x (%)	d (nm)	T_C (K)	M_S (emu/cm^3)	p (10^{21} cm^{-3})
F010	1.5	20	29	8.9	0.15
F007	2.5	20	60	11.5	-
F002	3	20	77	16.2	0.66
F016	3.8	20	96	24.7	-
E101	4.5	19	111	27.8	1.03
F020	5.2	20	132	333	1.08
D071	7	50	150	47.4	-
E115	7	20	159	51.0	1.41
E122	9	20	179	63.7	1.55
F056	14	20	182	78.1	1.81

Table 1: Table summarizing the basic characteristics of the $Ga_{1-x}Mn_xAs$ samples used in this thesis: x is the nominal Mn doping, d is the film thickness, T_C is the Curie temperature, M_S is the saturated magnetic moment and p is the hole concentration.

3. Static magneto-optics in (Ga,Mn)As

The interconnection between the magnetic, electric and optical effects in (Ga,Mn)As, together with the direct gap band structure, make this FM semiconductor an ideal system for investigating its basic properties by the optical spectroscopy. Moreover, in the presence of the ferromagnetic order, the spin degeneracy of the conductance and valence bands is removed (in analogy with the Zeeman splitting) [44], which gives rise to an appearance of the magneto-optical (MO) effects [50, 51, 52]. MO spectroscopy is extremely beneficial as it enables to study the electronic structure of DMS and it provides an insight into the exchange mechanism between the holes and the local magnetic moments. Moreover, the MO spectroscopy enables to discriminate between the intrinsic (induced by the Mn moments) and extrinsic (induced by the impurities or defects) origin of the FM phase [31, 53], so it is very convenient to use it as a complementary technique to the standard magnetization measurement techniques like SQUID. The most common MO effects, which are typically employed for the investigation of (Ga,Mn)As properties, are described in the following section.

The term "MO effects" comprises a large number of phenomena where the interaction of polarized light with a magnetized medium leads to a change of polarization state of the incident light [54]. The polarized light can be represented in orthogonal basis as a sum of two linear (*s* and *p*) or circular (σ^+ and σ^-) polarizations. The MO interactions lead to a change of the complex index of refraction ($\hat{n} = n + ik$) for two orthogonal polarizations and, consequently, the polarization of transmitted/reflected light is rotated and/or the ellipticity is changed. The polarization changes induced by the real part of the index of refraction cause a magnetic birefringence, whereas the imaginary part causes a magnetic dichroism [54]. Both effects are complementary and appear simultaneously because of the Kramers–Kronig relations between *n* and *k*.

MO effects can be sorted on the basis of the geometry between the incident light propagation (***k***) and the orientation of magnetization (***M***). In the case of normal incidence, with ***k*** parallel to ***M***, the energy levels are split into doublets (known as the longitudinal Zeeman effect) and the transitions between the spin-split levels and the ground state occur for σ^+ or σ^- [55]. The MO effects that appear in this configuration are odd functions of magnetization, i.e. they change sign when the magnetization orientation is reversed and they are proportional to the magnetization magnitude. These effects are also generally called as the first order MO effects. For ***k*** perpendicular to ***M***, the energy levels are split into triplets (known as the transversal Zeeman effect) and the middle and peripheral levels correspond to *s* and *p* linear polarizations, respectively [55]. The effects occurring in this geometry are even (quadratic) functions of magnetization, i.e. their sign is *not* changed when the magnetization direction is reversed and they are proportional to magnetization square. The effects in this geometry are also called as the second order or quadratic MO effects.

Since this thesis is focused on the study of (Ga,Mn)As properties by MO effects, the ones used in our experiments – the magnetic circular/linear dichroism and birefringence – are

briefly introduced. For simplicity, the transmission geometry and the normal incidence of light are considered in the following section.

Magnetic circular dichroism (MCD) is caused by a different absorption coefficient for σ^+ and σ^- circularly polarized light when $\boldsymbol{k}$ is parallel to $\boldsymbol{M}$. For linearly polarized incident light, $\boldsymbol{M}$ induces a change in the amplitude ratio between σ^+ and σ^-, which causes the rise of ellipticity (see Fig. 2a). The spectral dependence of MCD is essential for revealing the magnetic nature (i.e. antiferromagnetic or ferromagnetic) of the exchange interaction between the local Mn moments and the free carriers in (Ga,Mn)As [31, 32, 39]. Due to this feature, the MCD spectra were extensively studied in samples with different Mn doping and carrier concentrations, see e.g. Refs. 26, 32, 37, 53. The huge amount of the experimental results led to a dichotomy in the electronic band structure of (Ga,Mn)As, forming two competing theories – the VB and IB models (see Chap. 2.2). The IB model is promoted because of the observed rigidity of the near-band gap feature in the MCD spectra with increasing doping [26, 37], supported by the red-shift of the peak in the infrared (IR) absorption [38]. However, it was later shown by Jungwirth et *al*. (see Ref. 32 in Appendix 1), that this trend is not generic, as the blue-shift of the sharp MCD spectral feature at the band-gap energy (as well as the IR absorption peak) with increasing Mn doping was observed, in accordance with the predictions of the VB model with the AF *p-d* interaction. Despite the yet unsolved question about the character of the band structure in (Ga,Mn)As, the MCD spectroscopy proved to be a powerful tool for investigation of the intrinsic nature of FM in DMS.

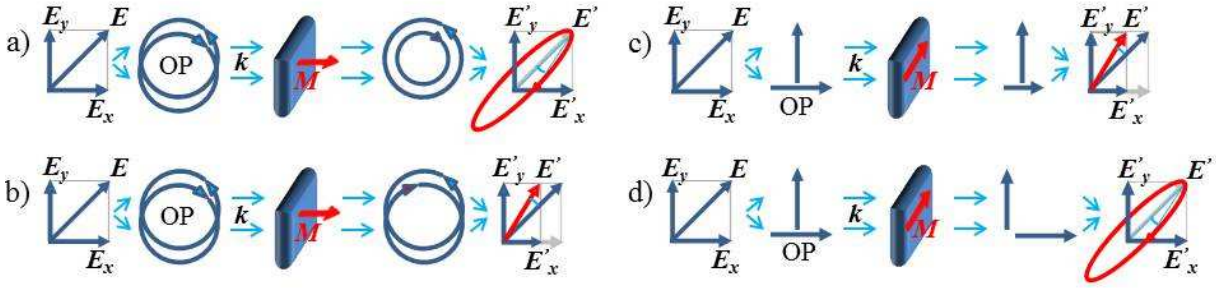

Fig. 2: Schematic illustration of magnetic circular dichroism (a), magnetic circular birefringence (b), magnetic linear dichroism (c) and magnetic linear birefringence (d). $\boldsymbol{E_x}$ and $\boldsymbol{E_y}$ are the *x* and *y* components of the incident light polarization $\boldsymbol{E}$ which is subsequently decomposed into two orthogonal polarizations (OP) in the given basis. The polarization of the transmitted light is changed after passing through the magnetized sample and the new polarization is depicted as $\boldsymbol{E}$'(with the $\boldsymbol{E}'_x$ and $\boldsymbol{E}'_y$ components). $\boldsymbol{M}$ represents the direction of magnetization and it is parallel to the incoming light direction ($\boldsymbol{k}$) in (a) and (b) and perpendicular to $\boldsymbol{k}$ in (c) and (d).

Magnetic circular birefringence (MCB) is a complementary effect to MCD, which is induced by a different index of refraction for σ^+ and σ^-. The difference in the refraction indices causes a phase shift between these two orthogonal polarizations, which in turn leads to rotation of the light polarization plane (see Fig. 2b). This effect is more commonly called the Polar Faraday or Kerr effect in transmission or reflection geometry, respectively. The static Polar Kerr effect (PKE) is widely used MO effect that is well established for probing the magnetic arrangement, FM interactions or the mechanisms of the magnetization reversals [53, 56, 57]. In addition, PKE is an AC-analogy to the anomalous Hall effect (AHE), as it is

directly proportional to the transversal component of conductivity (σ_{xy}), and can thus supplement the AHE measurements in the finite-frequency domain [53, 58]. PKE is also extensively used in the time-resolved MO measurements for observing the out-of-plane component of the magnetization dynamics, see e.g. Refs. 59, 60, 61 and the references therein.

Magnetic linear dichroism (MLD) is detected in a geometry when ***k*** is perpendicular to ***M*** and is caused by a difference in the absorption coefficient for *s* and *p* polarizations, resulting into rotation of the linearly polarized light (see Fig. 2c). This effect was found to be very small in conventional metals and was typically omitted in the studies of their MO properties [54, 62, 63]. In (Ga,Mn)As, however, a "giant" MLD signal was discovered recently [52, 64]. Its magnitude is spectrally dependent and it was found that it can even exceed the magnitude of PKE in some spectral regions, see e.g. Tesařová et *al*. in Refs. 65 and 66 (Appendices 2 and 5, respectively). Analogously to PKE, it can be perceived as the finite-frequency extension of the anisotropic magneto-resistance (AMR), and thus it can be exploited in elucidating the unclear origin of the AMR [67]. It was also shown that MLD is very valuable for a reconstruction of the real-space magnetization dynamics as it provides the access to the in-plane component of magnetization. For further analysis of the MLD see Chap. 4 or Tesařová et *al*. [66] in Appendix 5.

Magnetic linear birefringence (MLB) is a complementary effect to MLD. It is caused by a different index of refraction for *s* and *p* polarizations, which shifts their mutual phase and, consequently, it leads to the light elliptically change (see Fig. 2d).

It is important to note that such a simple and elegant division of the MO effects, based on the real and imaginary part of the complex index of refraction, is possible only in the transmission geometry. Although the manifestation of these effects stays the same in the reflection geometry, their origin might differ in such extent, that the change of the absorption and refraction index cannot be strictly separated [68]. In this thesis, all the mentioned MO effects were used mainly in the reflection geometry as an experimental tool for studying the manifestation of the FM order under different conditions, and, therefore, the exact origin of these MO effects was not of the fundamental importance.

In the following part of this thesis, we will show how the presented MO effects can be exploited in determining the basic material properties by other means than just the conventional measurements of the hysteresis loops or the MO spectra. The MO effects will be used in the time-resolved pump and probe spectroscopy (see Appendix 9) to study the magnetization dynamics. We show that this technique is not only favorable for determining the essential material parameters of (Ga,Mn)As but it also enabled us to reveal some new and intriguing physical phenomena in this material system.

4. Laser-induced precession of magnetization

The ever-increasing demand for speeding up the information storage and processing in the magnetic media leads to an intense research in fast manipulation of the magnetization state. While the transistor-based electronics is currently working in a few gigahertz clock-speed regime (~ 300 ps), the storage on magnetic hard discs, where the information is stored in magnetized domains (logic states "0" and "1" represent two different magnetization orientations), requires few nanoseconds, creating so called the ultrafast technology gap [69]. One of the alternatives to the magnetic field-induced magnetization switching is the current induced torque (CIT; also known as the spin transfer torque) [15]. The magnetization manipulation by CIT originates from the angular momentum transfer, where the magnetic layer orientation is flipped due to the angular momentum carried by the spin polarized current (see Chap. 5.2). The time scale of such CIT induced magnetization switching is on the order of several hundred picoseconds [70]. However, the observation of subpicosecond demagnetization by 60 fs laser pulses (in Ni films) [71] has opened a new perspective of the ultrafast magnetization manipulation by means of optics. Pumping the magnetic system with the optical laser pulses strongly disturbs the equilibrium between the lattice, carriers and magnetization [69, 72] and leads to several quasi-equilibrium dynamical processes that can provide insight into the strength and timescale of various microscopic interactions [72], or can reveal some new photoinduced phenomena, as will be discussed in more detail in Chap. 5.

The aim of the following chapters is to elucidate one of such dynamical processes – the laser pulse-induced magnetization precession – and to demonstrate the strength of the MO spectroscopy in determination of the real-space magnetization trajectory and in investigation of the basic material properties of (Ga,Mn)As. Moreover, we show how this experimental technique can be exploited in revealing new physical phenomena.

4.1 Magnetization dynamics observed by MO spectroscopy

The impact of a strong laser pulse induces a change of the equilibrium conditions between the reservoirs of spins, free carriers and phonons in the (Ga,Mn)As sample [73]. Because the magnetic properties of (Ga,Mn)As are strongly dependent on the interaction between the spins and charge carriers, the impact of the laser pulse induces a precession of magnetization (even if no external magnetic field is applied), which can be detected as an oscillatory MO signal. In (Ga,Mn)As the oscillatory motion of magnetization was for the first time observed in 2005 by Oiwa et *al*. [74]. Since then, the photoinduced magnetization dynamics in (Ga,Mn)As have been studied by many different groups, see e.g. Refs. 59, 60, 61, 75, 76 77, 78.

In these studies the observed MO signals were found to be independent of the excitation polarization, at least for time delays > 100 ps as can be seen from Fig. 3a. This indicated that the detected MO signal (rotation of the light polarization plane $\Delta\theta$) – that reflects the oscillations of FM coupled Mn spins – was not connected with the light angular momentum

transfer. The magnetic origin of the measured MO signal was further investigated by Tesařová et *al*. in Ref. 79 (see Appendix 3), where the pump-induced change of rotation ($\Delta\theta$) and ellipticity ($\Delta\eta$) were measured simultaneously (see Fig. 3b).

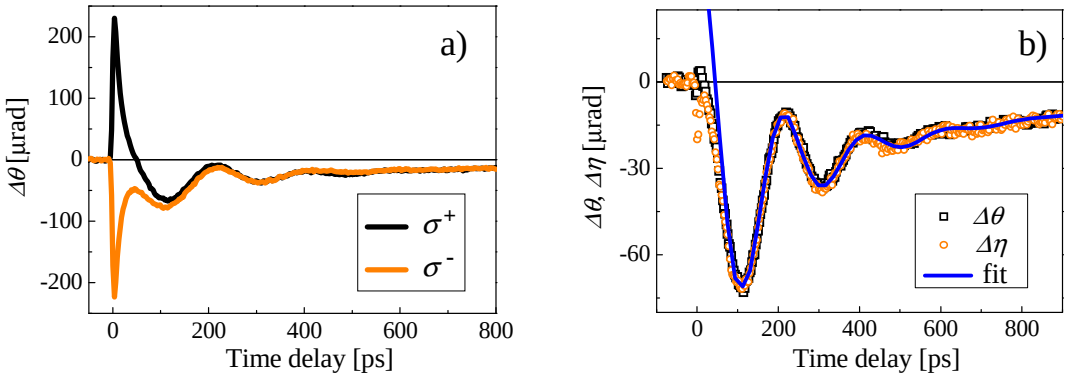

Fig. 3: MO signals measured as a function of time delay between pump and probe laser pulses. a) Dynamics of the probing light polarization rotation $\Delta\theta$ measured for two circular pump polarizations (σ^+ and σ^-). b) Polarization-independent part, $(\sigma^+ + \sigma^-)/2$, of the rotation ($\Delta\theta$) and ellipticity ($\Delta\eta$) (points) measured under identical conditions. The solid line corresponds to the fit by a damped harmonic function: $MO(\Delta t) = Acos(2\pi f\Delta t + \Phi)e^{-\frac{\Delta t}{t_G}} + Ce^{-\frac{\Delta t}{t_p}}$, where A = 82 μrad, t_G = 145 ps, f = 196.6 GHz, Φ = 59°, C = -42 μrad, t_p = 700 ps. Experimental data were taken for (Ga,Mn)As with 3% Mn concentration, at T = 15 K and with no external magnetic field applied. 80 fs pulses from the Ti:sapphire laser were tuned to 1.63 eV with pump intensity 46 μJcm^{-2}.

The data show similar behavior from time delays > 10 ps, confirming the FM origin of the measured MO signal at longer time scales and suggesting the non-magnetic (so-called optical) contribution right after the impact of the laser pulse [79, 80]. From the numerous experimental observations, it was concluded that the magnetization oscillations are caused by the laser-induced change of the magnetic anisotropy (MA), see e.g. Refs. 59, 76, 78. Since the MA is a function of *p*, *T* and strain, their slight photo-induced change influences the overall MA, thus the EA position of magnetization (see Chap. 2.3). However, the exact mechanisms of the anisotropy change remains an open question, where both the *thermal* (change in the sample temperature) and the *non-thermal* (change in the carrier concentration) origin of the MA change was considered [59, 61, 77]. The magnetization dynamics were investigated as a function of temperature [59, 61, 76, 78, 81], excitation intensities [24, 59, 61, 76, 78] and energies [80], carrier concentrations [24, 61, 78] or thermal annealing [61], but the experimental observations obtained by different groups led to ambiguous interpretations of the magnetization dynamics origin [24, 61, 76, 77]. We note that the diversity may come from the distinct quality of the studied samples. As mentioned above (in Chap. 2.3), (Ga,Mn)As is a highly disordered material system and its magnetic properties depend on various parameters, such as growth conditions, film thickness, post-growth treatment and so on. All these factors may lead to different observations of the magnetization dynamics, even at similar experimental conditions. The latest studies of Tesařová et *al*. in Ref. 24 (see Appendix 7) on a high quality samples suggest, that in principle, both mechanisms (thermal and non-thermal) are present and are not easily distinguishable. It was shown, that at lower excitation intensities

(I < 70 μJcm^{-2}), the thermal mechanism prevails, but for higher intensities, the temperature increase is saturated and the magnetization dynamics is dominated by the non-thermal effects (see Chapter 5 for detailed discussion). Nevertheless, it was also found that the impact of the laser pulse does not always lead to the precession of magnetization (see Appendix 4) [82]. In samples with strong uniaxial (i.e. the EA oriented in [-110] crystallographic direction), or cubic anisotropy (i.e. the EA oriented in [100] or [010] crystallographic direction), no magnetization oscillations were observed – at least for the excitation intensities I < 28 μJcm^{-2} – as the impact of the laser pulse is not sufficient to reorient the equilibrium EA position. It was concluded that the laser-induced change of the EA, which triggers the magnetization dynamics, can be observed only in samples where the cubic and uniaxial anisotropies are "comparable", so that the equilibrium EA is oriented between [010] and [-110] crystallographic directions. Moreover, it was shown that the MA has a strong influence not only on the precessional frequency (as will be discussed in Chap. 6), but also on the amplitude of the oscillations, as observed by Tesařová et *al*. in Ref. 82 (see Appendix 4 for further details).

The measured data of magnetization precession can be phenomenologically fitted by a sum of damped harmonic function and a non-oscillatory pulse-like background function [59, 60, 66]:

$$MO\ (\Delta t) = Acos(2\pi f \Delta t + \Phi)e^{-\frac{\Delta t}{t_G}} + Ce^{-\frac{\Delta t}{t_p}}, \quad (2)$$

where A and C are the amplitudes of the harmonic and pulse-like functions, respectively, f is the frequency of precessing Mn spins, Φ is an initial phase, t_G is the Gilbert damping time (see Chap. 6), and t_p is the damping time of the pulse-like function. As seen from Fig. 3b, only the quasi-equilibrium part of the MO signal, reflecting the precessional motion of magnetization, can be fitted well by Eq. 2. In fact, this formula describes a phenomenological model, in which the MO signal can be decomposed into the damped magnetization oscillations around the quasi-equilibrium EA and the laser-induced tilt of the equilibrium EA position [Supplementary material in 21, 82].

The situation can be in more detail described as the following: Before the impact of the laser pulse, the magnetization is aligned with the equilibrium EA, given by the free energy minimum (see Fig. 4a and Eq. 1 in Chap. 2.3). The impact of the laser pulse changes the overall MA, which leads to the shift of the EA (Fig. 4b). At this moment, the instant position of magnetization and the EA are not aligned, so the magnetization starts to approach the transient EA position by an oscillatory motion, which can be perceived as the precession of magnetization around some inherent effective magnetic field [77, 81]. As the laser-induced changes are decaying, the transient EA is returning to its equilibrium position and the precession of magnetization is damped by the Gilbert damping at the same time (Fig. 4c).

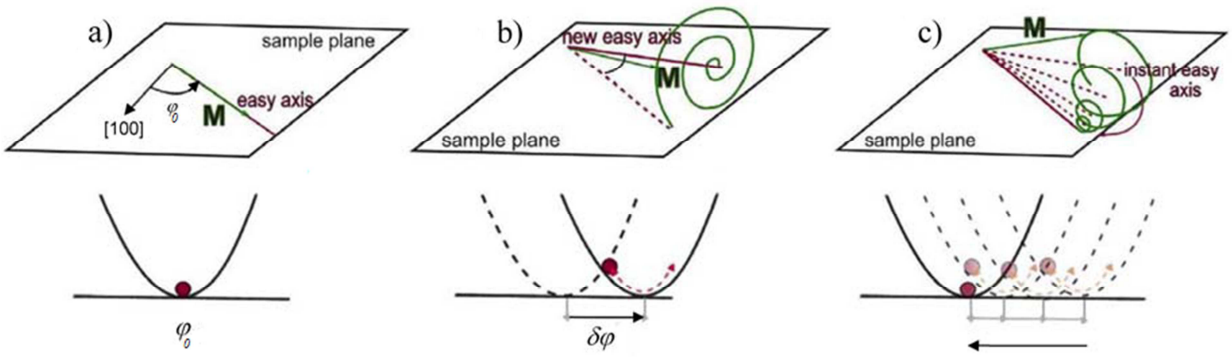

Fig. 4: Schematic illustration of the pulse-induced precession of magnetization. a) In equilibrium, the magnetization is aligned with the EA position, which lies in the sample plane at the angle φ_0 from the [100] crystallographic direction. b) The impact of a strong laser pulse induces a transient change of the MA, which leads to the reorientation of the easy axis and subsequently to the precession of magnetization. c) The recombination of the photoinduced carriers and the heat dissipation slowly restore the equilibrium conditions, making the EA return to its original position. Simultaneously, the magnetization precession in damped by the Gilbert damping. [43]

The anisotropy-dependent precession of magnetization can be of a practical use as it can be controlled by external means – either optically by another laser pulse [60], or electrically by a piezo-transducer [21]. The electrical control by piezo-stressing allows the manipulation of the overall strain in the sample, which enables either to enhance or completely suppress the magnetization dynamics, see Ref. 21 in Appendix 6. We note that the laser-induced magnetization precessions can be also used for determination of the basic properties of (Ga,Mn)As, such as the MA constants K_i, the Gilbert damping constant α, or the spin stiffness parameter D (as will be discussed in detail in the Chap. 6) – in a way rather similar to ferromagnetic resonance experiments [FMR]. Before proceeding to such specific characteristics of (Ga,Mn)As, let's have a closer look at the real-space magnetization trajectory after the impact of the laser pulse.

4.2 Real-space magnetization dynamics

MO spectroscopy is a very powerful tool for the investigation of the magnetization trajectory in the real space as it reflects both the in-plane and out-of-plane motion of magnetization sensed by MLD and PKE, respectively. In order to separate these two contributions in the measured MO signals, their distinct polarization dependences can be used as will be demonstrated in the following sections. The polarization dependence of PKE and MLD will be derived first for the static MO signals and, subsequently, it will be applied to the analytical model of magnetization dynamics described by Eq. 2. We stress that the detailed understanding of the measured dynamical MO signal, together with the polarization dependence of PKE and MLD, enables to perform a full quantitative 3D reconstruction of the magnetization precessional motion without any numerical modeling.

4.2.1 Polarization dependence of static MO signal

As mentioned in Chap. 3, there are four different MO effects that can change the polarization state of light when reflected from the magnetized media (taking just the reflection geometry with small angles of incidence into account). In the following discussion, the polarization dependence of only two of them, causing the *rotation* of the light polarization plane, will be investigated – PKE (sensitive to out-of-plane projection of ***M***) and MLD (sensitive to in-plane projection of ***M***), but the obtained results can be also applied for MCD and MLB, causing the light ellipticity change. In general, the orientation of magnetization can be characterized by the polar and azimuthal angles φ_0 and θ_0, respectively (see Fig. 5a for the angle definition). In the case of PKE, the rotation of light polarization ($\Delta\beta$) is proportional to the projection of magnetization to the direction of light propagation and it is insensitive the incident polarization orientation (see Figs. 5b and 2b):

$$\Delta\beta^{PKE} = \beta' - \beta = P^{PKE} cos\theta_0, \tag{3}$$

where P^{PKE} is the corresponding MO coefficient of the sample, which can be measured when the magnetization is oriented by a strong external magnetic field out of the sample plane (θ_0 = 0˚).

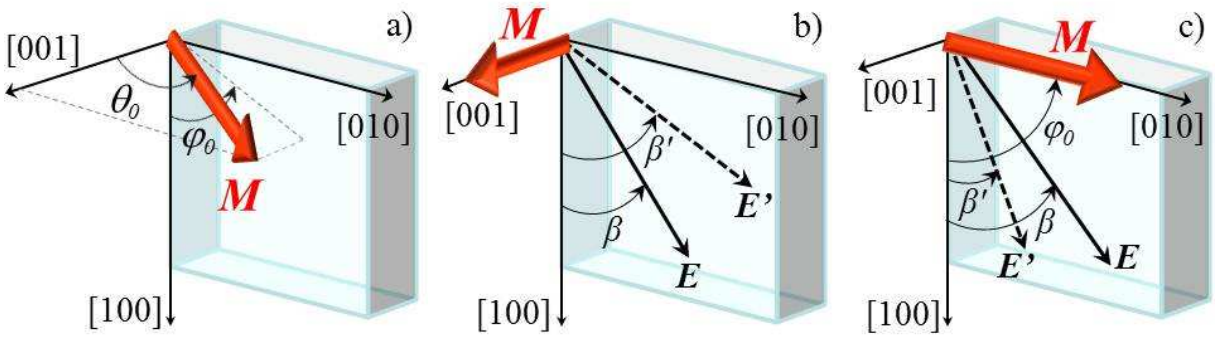

Fig. 5: a) Definition of the polar angle φ_0 and azimuthal angle θ_0, that determine the position of magnetization ***M*** in the sample. b) Rotation of light polarization plane $\Delta\beta$ due to PKE, which is proportional to the out-of plane orientation of magnetization. PKE does not depend on the incident light polarization β. c) Rotation of the light polarization plane $\Delta\beta$ due to MLD, which is sensitive to in-plane position of ***M*** and depends on the incident light polarization orientation β; $\Delta\beta^{MLD} = P^{MLD} sin2(\varphi_0 - \beta)$. The incident polarizations are labeled ***E*** and the transmitted/reflected polarizations are labeled ***E'*** in b) and c), respectively.

In the case of MLD, the rotation of light polarization is proportional to the projection of magnetization to the direction perpendicular to light propagation (see Fig. 2c) and it strongly depends on the incident polarization orientation β. The polarization dependence of the MLD can be analytically calculated using the trigonometric relation between the magnetization orientation in the sample plane, given by the angle φ_0, and the incident and reflected light polarizations, given by the angles β and β' (see Fig. 5c and Ref. 65 in Appendix 2 for more details):

$$\Delta\beta^{MLD} = \beta' - \beta = P^{MLD} sin[2(\varphi_0 - \beta)], \tag{4}$$

where P^{MLD} is the MO coefficient defined as $P^{MLD} = 0.5(r_{\parallel}/r_{\perp} - 1)$ and $r_{\parallel}$ ($r_{\perp}$) describes the reflection coefficients for light polarized parallel (perpendicular) to magnetization orientation, respectively. Eq. 4 shows, that the polarization rotation $\Delta\beta$ due to MLD is maximized when the angle between $\boldsymbol{M}$ and the incident polarization orientation is ±45˚. In this case $\Delta\beta$ is given solely by P^{MLD}, thus this geometry is also used in order to determine the magnitude of P^{MLD} (the position of magnetization is fixed by a strong magnetic field). On the other hand, $\Delta\beta$ is zero when the incident polarization is parallel or perpendicular to $\boldsymbol{M}$ (i.e., $\varphi_0 - \beta$ = 0˚ or 90˚, respectively). In more general case, when the magnetization is not oriented in the sample plane, but has an arbitrary orientation given by φ_0 and θ_0, the polarization rotation due to MLD can be written as:

$$\Delta\beta^{MLD} = P^{MLD} sin^2\theta_0 sin[2(\varphi_0 - \beta)], \tag{5}$$

The overall rotation of light polarization is given by the sum of PKE and MLD contributions $\Delta\beta^{PKE}$ and $\Delta\beta^{MLD}$, respectively:

$$MO^{stat} = \Delta\beta^{PKE} + \Delta\beta^{MLD} = P^{PKE} cos\theta_0 + P^{MLD} sin^2\theta_0 sin[2(\varphi_0 - \beta)]. \tag{6}$$

It is important to note that since PKE is a first-order MO effect, P^{PKE} is directly proportional to magnetization magnitude M_0 (provided that $\boldsymbol{M}$ is oriented along the direction of light propagation). On the other hand, MLD is a second-order MO effect (or quadratic MO, see Chap. 3) and thus the P^{MLD} depends quadratically on M_0, i.e. $P^{MLD} \sim M_0^2$ (provided that $\boldsymbol{M}$ is oriented perpendicular to the direction of light propagation).

4.2.2 Dynamical MO signal in (Ga,Mn)As and its polarization dependence

As mentioned above, the impact of the laser pulse modifies the anisotropy of the sample, which shifts the equilibrium position of the EA, that subsequently leads to the precession of magnetization. The oscillatory motion of magnetization can be detected as a dynamical MO signal δMO that is strongly dependent on the incident light polarization, see Tesařová et *al*. [66] in Appendix 5. To express this explicitly, the analytical formula describing the magnetization dynamics (Eq. 2) can be rewritten in the following form:

$$\delta MO\ (\Delta t, \beta) = A(\beta) cos[2\pi f \Delta t + \Phi(\beta)] e^{-\frac{\Delta t}{t_G}} + C(\beta) e^{-\frac{\Delta t}{t_p}}, \tag{7}$$

where the meaning of the particular components remain the same as in Eq. 2. Moreover, the polarization dependence of the oscillatory and pulse-function amplitude [$A(\beta)$ and $C(\beta)$] enables more thorough insight into the character of the magnetization dynamics and a direct determination of the EA position.

Firstly, the pulse-like function in δMO signal describes the transient non-oscillatory change of the static MO signal MO^{stat}. In fact, in this signal there are two contributions that are reflecting different origin of the magnetization dynamics. The first one reflects the magnetization dynamics due to the *tilt* of the equilibrium EA position, which can be described

as a derivative of Eq. 6 with respect to small change of φ and θ. The second one is connected with the laser-induced change of the magnetization magnitude (*demagnetization*), due to the laser-induced heating of the sample, and can be also obtained from the derivative of Eq. 6 with respect to magnetization change (through the dependence of P^{PKE} and P^{MLD} on the magnetization magnitude). Taking into account that all the samples investigated in this thesis are in-plane magnets, i.e. $\theta_0 = 90^\circ$, we obtain the following expression for the measured pulse-like function amplitude $C(\beta)$:

$$C(\beta) = C_{tilt}(\beta) + C_{demag}(\beta) = \\ -\delta\theta_{qe}P^{PKE} + \delta\varphi_{qe}P^{MLD}2cos\,2(\varphi_0 - \beta) + \frac{\delta M}{M_0}P^{MLD}2sin\,2(\varphi_0 - \beta), \qquad (8)$$

where the first two terms on the right-hand side correspondent to $C_{tilt}(\beta)$ and the last term corresponds to $C_{demag}(\beta)$. $\delta\varphi_{qe}$ and $\delta\theta_{qe}$ describe the transient in-plane and out-of-plane tilt of the EA position and $\delta M/M_0$ describes the reduction of the magnetization magnitude (relative to the equilibrium value M_0). Eqation 8 is of high importance as it directly determines whether the magnetization precession is triggered by the in-plane or out-of-plane tilt of the EA. In the case of the in-plane tilt of the EA, the polarization dependence of C_{tilt} is given by the *cos*-like harmonic function. On the other hand, if the EA is tilted out-of plane, C_{tilt} does not depend on the incident light polarization β. In the case when the EA is tilted in a general direction, C_{tilt} depends harmonically on β, but there is an offset in the polarization dependence. Moreover, fitting the polarization dependence $C(\beta)$ by Eq. 8 enables to quantify the EA tilt, see Tesařová et *al*. [66] in Appendix 5.

The oscillatory function in δMO signal describes the precessional motion of magnetization around the transient EA position and it naturally consists of the in-plane and out-of-plane contributions sensed by MLD and PKE, respectively. The oscillatory function amplitude $A(\beta)$ can be thus written is the form:

$$A(\beta) = \sqrt{[A^{MLD}(\beta)]^2 + [A^{PKE}]^2}, \qquad (9)$$

where $A^{MLD}(\beta)$ describes the β-dependent MO amplitude due to the in-plane motion of magnetization and A^{PKE} is the out-of plane contribution of the precessional amplitude which does not depend on β. The analytical formula for A^{MLD} and A^{PKE} can be obtained from Eq. 6 as its derivative with respect to in-plane and out-of-plane angles φ and θ. Moreover, if we consider that the initial amplitude of the oscillations is approximately equal to the EA tilt $\delta\varphi_{eq}$ and $\delta\theta_{eq}$, the overall oscillatory amplitude is given as:

$$A(\beta) = \sqrt{\left[\delta\varphi_{qe}P^{MLD}2cos\,2(\varphi_0 - \beta)\right]^2 + [-\theta_{qe}P^{PKE}]^2}\,. \qquad (10)$$

The polarization dependence of the oscillatory amplitude is crucial for determining the equilibrium position of the EA in the sample plane, φ_0 (and thus the magnetization position before the impact of the laser pulse). φ_0 corresponds to the polarization orientation where the dependence $A^{MLD}(\beta)$ shows the maximum (see also Fig. 11b below). This conclusion is obvious from the fact, that $A^{MLD}(\beta)$ describes the change of the static MO signal $\Delta\beta^{MLD}$, which

is the strongest when the incident polarization is aligned parallel (or perpendicular) with the magnetization position, i.e. $\beta = \varphi_0$ (or $\beta = \varphi_0 \pm 90^\circ$), see Tesařová et *al*. [66] in Appendix 5.

4.2.3 Reconstruction of magnetization real-space trajectory

The detailed understanding of the time-dependent MO signal enables to perform a quantitative reconstruction of the magnetization real-space trajectory directly from the measured MO signals without assuming any theoretical model or any fitting parameter. As was already mentioned, prior to the impact of the laser pulse, the magnetization is aligned with the EA position (described by φ_0 and θ_0). The impact of the pump pulse disturbs the equilibrium conditions in the sample and leads to the magnetization precession, which is detected by the time-delayed probe pulses. The instantaneous position of the magnetization can be described by the polar and azimuthal angles φ and θ:

$$\varphi(\Delta t) = \varphi_0 + \delta\varphi(\Delta t), \tag{11a}$$

$$\theta(\Delta t) = \theta_0 + \delta\theta(\Delta t), \tag{11b}$$

where $\delta\varphi(\Delta t)$ and $\delta\theta(\Delta t)$ describe the time-dependent in-plane and out-of-plane movement of magnetization, respectively. The magnetization dynamics changes the static MO signal MO^{stat} and the measured MO signal can be thus expressed in terms of the instantaneous magnetization position as a derivative of Eq. 6 with respect to φ, θ and M_0:

$$\delta MO(\Delta t, \beta) = \\ -\delta\theta(\Delta t) P^{PKE} + \delta\varphi(\Delta t) P^{MLD} 2cos\,2(\varphi_0 - \beta) + \frac{\delta M}{M_0} P^{MLD} 2sin\,2(\varphi_0 - \beta), \tag{12}$$

where the first two terms are connected with the oscillatory movement of magnetization and the last term is connected with the demagnetization. We note that Eq. 12 is derived for the in-plane position of the EA, which is the case for all the (Ga,Mn)As samples measured in this thesis. The polarization dependence of the measured MO signal $\delta MO(\Delta t, \beta)$ enables to separate the in-plane and out-of-plane motions of the magnetization, sensed by MLD (which is sensitive to β) and PKE (which is not sensitive to β), respectively. It is apparent from Eq. 12 that the in-plane motion of magnetization can obtained as a linear combination of the MO signals measured for $\beta = \varphi_0$ and $\varphi_0 - 90^\circ$ because the in-plane motion of magnetization is maximal and exactly opposite for $\beta = \varphi_0$ and $\varphi_0 - 90^\circ$ and the demagnetization does not contribute to the measured signal for these angles β. Consequently,

$$\delta\varphi(\Delta t) = [\delta MO(\Delta t, \varphi_0) - \delta MO(\Delta t, \varphi_0 - 90°)]/(4P^{MLD}). \tag{13}$$

Similarly, the out-of-plane motion and the demagnetization can be calculated for $\beta = \varphi_0 - 45^\circ$ and $\varphi_0 - 135^\circ$, where the contribution due to the in-plane motion $\delta\varphi$ does not contribute and the demagnetization terms are exactly opposite:

$$\delta\theta(\Delta t) = -[\delta MO(\Delta t, \varphi_0 - 45°) + \delta MO(\Delta t, \varphi_0 - 135°)]/(2P^{PKE}), \tag{14}$$

$$\frac{\delta M(\Delta t)}{M_0} = [\delta MO(\Delta t, \varphi_0 - 45°) - \delta MO(\Delta t, \varphi_0 - 135°)]/(4P^{MLD}) \quad (15)$$

We note, that also other linear combinations of the $\delta MO(\Delta t, \beta)$ are in principle possible in order to obtain $\delta\varphi(\Delta t)$, $\delta\theta(\Delta t)$ and $\delta M(\Delta t)/M_0$. However, the presented Eqs. 13, 14 and 15 are the most simple and straightforwardly describe the magnetization dynamics after the impact of the laser pulse. In any case, the quantitative reconstruction of the in-plane and the out-of-plane real-space magnetization trajectory depends solely on the signals δMO, which are measured for different probe polarizations β, and on the magnitude of the MO coefficients P^{MLD} and P^{PKE}, which are determined independently in the static MO experiments (see Chap. 4.2.1). The examples of the magnetization dynamics calculated by this procedure can be found in Refs. [66] (see Appendix 5), [21] (see Appendix 6) and [24] (see Appendix 7).

5. Origin of magnetization precession

As pointed out in the previous chapter, the origin of the light-induced precession of magnetization in (Ga,Mn)As is a widely discussed issue, where two distinct mechanism of MA change – the thermal and the non-thermal – are considered to be responsible for this phenomenon [59, 61, 74, 76, 77]. The non-thermal origin was firstly suggested by Oiwa et *al*. [74] and subsequently followed by Hashimoto et *al*. [77]. The authors claimed that the variation of the MA is driven by the generation, cooling and subsequent annihilation of the photo-generated holes. They estimated the relative increase in the hole concentration to be ~ 0.01% for the excitation fluence of ~ 3 μJcm^{-2} [77]. On the other hand, Qi et *al*. [61] observed the magnetization precession for similar light intensities (~ 1 – 10 μJcm^{-2}) but it was ascribed to the transient change of temperature because its relative change was found to be 3 – 4 orders of magnitude larger than the hole concentration change. A new light into this issue is brought by the recent paper of Tesařová et *al*. [24] (see Appendix 7), which represents a thorough study of light-induced magnetization dynamics for a broad range of excitation intensities (~ 7 – 260 μJcm^{-2}). It is shown that, in principle, *both* mechanisms can lead to magnetization dynamics. Moreover, it is possible to separate the thermal and the non-thermal mechanisms by the real-space magnetization trajectory reconstruction (see Chap. 4) and to quantify the experimental conditions for which either of the mechanisms dominates.

In this chapter we discuss the thermal and the non-thermal origin of the oscillatory motion of magnetization in detail. In addition, we describe two distinct non-thermal mechanisms that can lead to magnetization precession.

5.1 Thermal origin

The impact of the laser pulse on (Ga,Mn)As sample (with the photon energy exceeding the energy of the band gap; E_g ~ 1.5 eV) leads to an instant generation of the electron-hole pairs, where the concentration of the photoinduced holes (δp) and electrons (δn_e) is equal. The scattering processes among the carriers build up a hot carrier Fermi-Dirac distribution on the sub-picosecond time scale [61]. Subsequently, the carriers recombine non-radiatively (because of the high concentration of the non-radiative recombination centers caused by the low-temperature growth by MBE; see Chap. 2.3) which increases the density of phonons due to the carrier-phonon interactions. The initial carrier energy is thus transferred to the lattice, resulting into a local increase of the temperature within a few picoseconds [59, 79]. The accumulated heat than diffuses from the illuminated area towards the equilibrium conditions on the time scale of hundreds of picoseconds [24]. The temperature raise time can be obtained directly from the differential reflectivity measurements ($\Delta R/R$) that provide information about the photo-injected carrier concentration and life-time (electrons in particular) [83], see Fig. 6a. The schematic picture of the temperature increase (δT) is depicted in Fig. 6b.

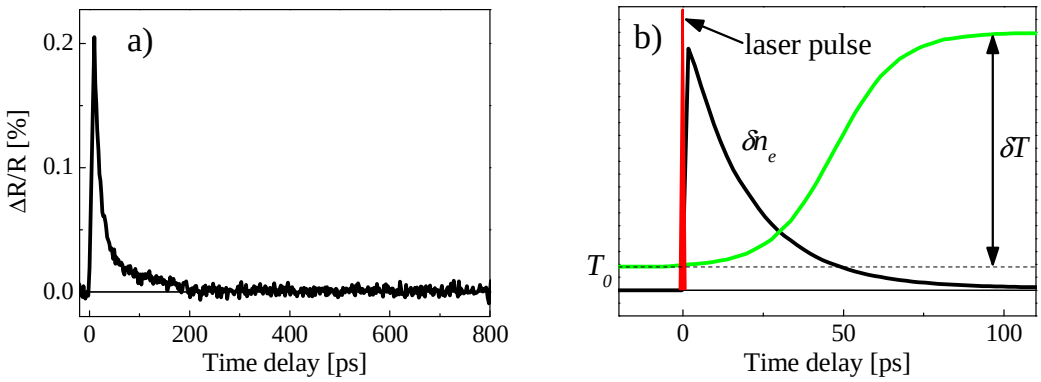

Fig. 6: a) Dynamics of the pump pulse-induced change of the sample reflectivity measured for (Ga,Mn)As sample with 3% Mn doping and the pump intensity I = 42 μJcm^{-2}. The reflectivity dynamics provide the information about the laser-induced carrier concentration (amplitude of the $\Delta R/R$) and lifetime (defined as a time where the reflectivity amplitude decreases to 1/e). b) Schematic illustration of the laser-induced change of the electron concentration (δn_e) and the subsequent temperature increase (δT) from the equilibrium temperature T_0 after the impact of the femtosecond laser pulse (red peak). The dynamics of δn_e is obtained from the measured transient reflectivity data shown in a) where the corresponding lifetime is ~ 20 ps.

The magnetic anisotropy constants are strongly dependent on the magnetization magnitude - the uniaxial anisotropy scales with magnetization magnitude as M^2 while the biaxial component scales as M^4. Consequently, when the temperature of the sample is increased (i.e., when the magnetization magnitude is decreased), the biaxial anisotropy is reduced more than the uniaxial one, causing the shift of the EA towards the [-110] crystallographic direction [41, 46]. The character of the subsequent magnetization precession around the new quasi-equilibrium EA position is unambiguously described – by the Landau-Lifshitz-Gilbert equation (LLG, see Chap. 6) – enabling the *initial* tilt of the magnetization only towards the [00-1] crystallographic direction. An estimate of the temperature increase δT can be done from the magnetization precession frequencies, as their magnitude reflects the temperature dependent magnetocrystalline anisotropies (see Chap. 6). Figure 7a shows the precession frequency (f) dependence on the sample temperature, measured for low excitation intensity I = 7 μJcm^{-2}, and on the excitation intensity for low sample temperature T = 15 K. The temperature increase δT as a function of the intensity can be deduced from the comparison of these two dependencies ($f(T)$ and $f(I)$) and is shown in Fig. 7b.

It is obvious from Fig. 7b that δT gets saturated around I = 70 μJcm^{-2}, but the character of the magnetization precession does *not* remain the same and changes dramatically for I > 70 μJcm^{-2}. More specifically, the initial tilt of the magnetization reverses towards [001] crystallographic direction for excitation intensities I > 70 μJcm^{-2} (see Tesařová et *al.* [24] in Appendix 7), which is not possible in the case of thermally-induced magnetization precession. Fig. 7b also shows that despite the saturated temperature increase, the hole concentration (δp) increases further with the increasing laser intensity [24]. We note, that δp and its intensity dependence can be calculated from the energy absorbed from the laser light (assuming the absorption coefficient of GaAs) and the intensity dependence of the $\Delta R/R$ amplitude (since δp = δn_e after the impact of the laser pulse). The thermally inaccessible tilts of magnetization for

$I > 70\ \mu\text{Jcm}^{-2}$, together with the increasing carrier concentration points to a distinct, non-thermal mechanism of the magnetization precession.

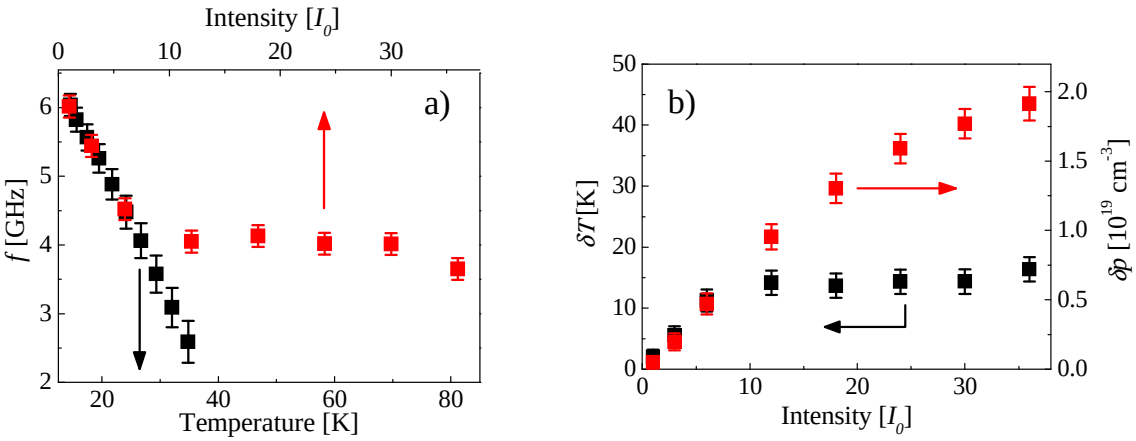

Fig. 7: a) Frequency of the magnetization precession as a function of the temperature (for $I_0 = 7\ \mu\text{Jcm}^{-2}$) and the excitation intensity (at sample temperature $T = 15$ K). b) The intensity dependence of the temperature increase (δT) and the excess hole concentration (δp) after the impact of the laser light. Experimental data were taken for (Ga,Mn)As sample with 3% Mn concentration.

5.2 Non-thermal origin

The non-thermal processes that lead to magnetization precession are caused by the photo-induced carriers and can be divided, regarding the polarization of the excitation light, into two groups – the polarization independent and the polarization dependent ones. In the later ones, the circularly polarized light generates carriers with the defined spin orientation [34] and the subsequent magnetization precession is caused by a transfer of the spin angular momentum from the photo-carriers to the magnetization. This effect, known as the optical spin transfer torque (OSST), was theoretically predicted several years ago [84], but it was experimentally observed only recently (by Němec et *al*. [21], see Appendix 6). On the other hand, the polarization independent processes can be observed for any polarization of light (i.e., also for the linearly polarized light). In this case, the magnetization precession occurs as a result of the carrier spin polarization caused by the relativistic spin-orbit coupling (SOC) among the photo-induced carriers in the spin-split energy band. The effect is called the optical spin-orbit torque (OSOT) and was for the first time ever observed by Tesařová et *al*. in [24] (see Appendix 7). Both of these non-thermal processes are described in more detail in the following sections.

5.2.1 Optical spin-orbit torque

The current induced spin-orbit torques (SOT), that were recently observed in (Ga,Mn)As, opened a new possibilities for further technological development, such as the extension of the operational capabilities in the electronic devices, or the unprecedented

characterizing techniques in material research [23, 85]. The OSOT is its optical analogue and it enables studying the magnetization-related phenomena on the time scales which are orders of magnitudes shorter than in the current induced SOT. This effect is based on the EA reorientation due to the optically induced change of the carrier concentration (holes in particular, since the electrons are weakly spin-orbit coupled) [24]. However, the reorientation of the EA and the subsequent initial tilt of magnetization can be in the opposite direction than in the case of the thermal mechanism, i.e. EA rotates towards the [010] and the magnetization tilts towards [001] crystallographic directions, respectively (compare with the thermal mechanism in Chap. 5.1). We note that the distinct character of magnetization dynamics, which can be determined from the analysis of magnetization real-space trajectory (described in Chap. 4), represents a straightforward method how to distinguish between the thermal and the non-thermal origin of magnetization precession. Such a simplified picture of the non-thermally induced oscillations of magnetization are in agreement with the theoretical calculations (based on the ***k.p*** kinetic exchange Hamiltonian) of the hole-concentration dependent EA position [41], but the detailed understanding of this effect requires more rigorous explanation, based on the SOC in the valance band.

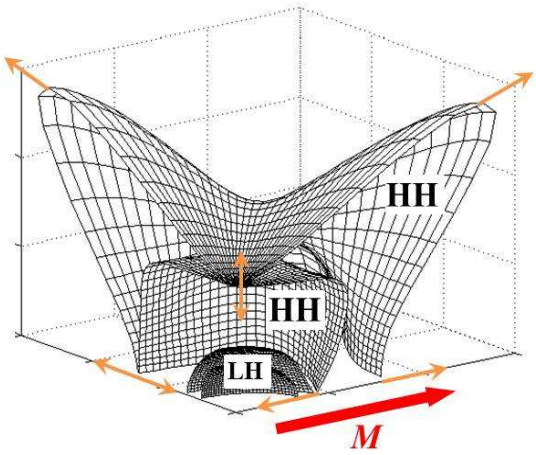

Fig. 8: Schematic illustration of the cross section of the Fermi volume in (Ga,Mn)As in the *k*-space. Non-zero magnetization (red arrow) leads to the anisotropic splitting of the valence bands into four subbands, two heavy (HH) and light (LH) holes bands. The direction of the hole spin orientation in different states on the Fermi surface is indicated by the orange arrows. [25]

Figure 8 shows the (Ga,Mn)As valance band (VB), where the magnetization leads to the anisotropic splitting of the VB into four bands – the spin-split heavy (HH) and light (LH) holes bands, respectively [25]. The SOC causes the change of the expected spin orientation along the top of the Fermi surface, which is essential for the occurrence of the magnetization torque and can be described as following. The impact of the linearly polarized laser light induces a non-equilibrium hole population. Since the angular momentum of light is zero, there is no momentum that could be transferred into the system, so the excited holes are not spin-polarized. However, the subsequent relaxation towards the spin-split Fermi sea of the equilibrium holes produces a non-equilibrium spin polarization, which is misaligned with the magnetization orientation. This photo-hole polarization can be perceived as an effective magnetic field that exerts a torque on the magnetization via the kinetic exchange coupling and leads to magnetization precession. It is important to note that in the case of *no* SOC, the only polarization that the holes could acquire would be parallel with magnetization orientation, which would exclude the existence of the torque. Despite the relatively simple physical origin of the OSOT, its quantitative description, involving the estimate of the hole polarization, is a

rather challenging problem. The exact theoretical treatment is complicated by the vast number of the non-equilibrium processes on the time scale of 10 – 100 femtoseconds after the impact of the laser pulse, that can influence the spin hole polarization before it is determined by the SOC. However, in the first approximation, the spin polarization of holes can be associated with the magnetic anisotropy field H_{an} [24]. In this approximation, the misalignment of the magnetization and the hole polarization has the same physical origin as the dependence of the magnetic EA orientation of the hole density [41].

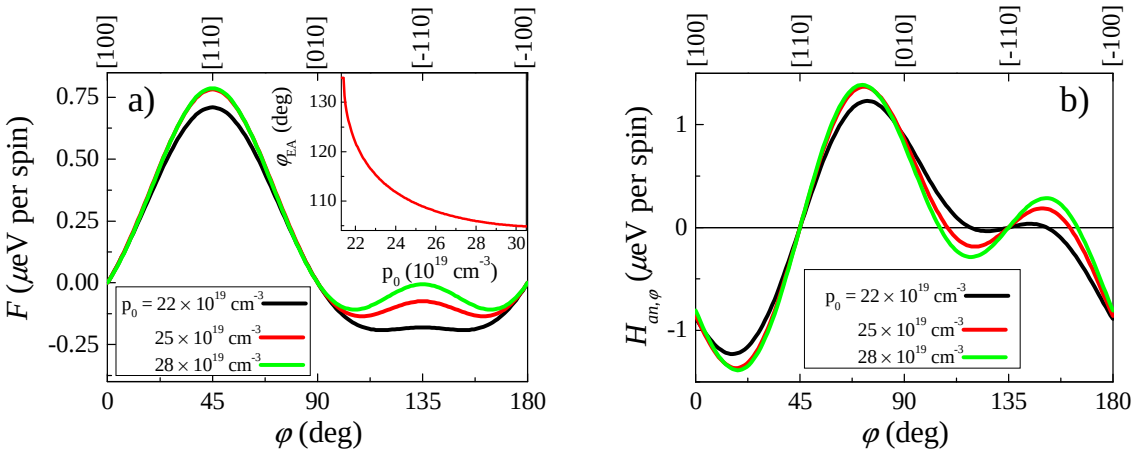

Fig. 9 Computed in-plane angular dependence of the free energy functional F (with respect to the energy along the crystallographic direction [100]) a) and the magnetic anisotropy field $H_{an,\varphi} = -\delta F/\delta\varphi$ b) in (Ga,Mn)As for different hole concentrations p_0. Inset: Dependence of the easy axis position on the concentration of holes. [Supplementary material in 24]

Figure 9a shows the in-plane dependence of the free energy functional F (see Chap. 2.3) in (Ga,Mn)As calculated for the different hole concentrations, where the minimum of F represents the equilibrium EA position (shown in the Inset). The impact of the laser pulse causes an increase of the hole concentration δp (with respect to hole concentration p_0 in dark), which leads to the in-plane movement of the EA and, consequently to the misalignment of the EA position and the magnetization orientation. These changes of the magnetic order give rise to the appearance of H_{an} ($H_{an,\theta} = -\partial F/\partial\theta$ and $H_{an,\varphi} = -\partial F/\partial\varphi$, see Ref. 24), which is non-zero in the plane of the sample (see Fig. 9b). The sign of the calculated H_{an} is consistent with the sense of the initial magnetization tilt observed in the experiments. The detailed derivation of the H_{an}, together with the additional analysis of the magnetization trajectory can be found in Ref. 24 (see Appendix 7).

5.2.2 Optical spin-transfer torque

The optical spin-transfer torque (OSTT) represents another non-thermal effect responsible for the magnetization dynamics after the impact of the laser light. Similarly to the OSOT, the magnetization oscillations are caused by the spin-momentum transfer from the carriers to the magnetization via the exchange coupling. The main difference between these two effects is that in the case of OSTT, the carriers acquire their spin polarization directly

from the circularly polarized light (and thus no SOC is needed for observing this effect). The detailed theoretical description of OSTT is given in Ref. 21 (see Appendix 6) and only a brief summary of this effect will be given here.

The circularly polarized light generates the spin-polarized carriers ($\delta n_e = \delta p < p_0$), where the carrier spin orientation (***n***) is parallel with the direction of the incident light and perpendicular to magnetization orientation (in the case of typical, compressively strained (Ga,Mn)As samples with the in-plane equilibrium position of ***M***), see Fig. 10. The appearance of the OSTT is conditioned by the relatively long spin lifetime of the photo-injected carriers [21] and only the photo-electrons spin lifetime of ~ 10 ps, which is given mainly by the interaction with Mn moments and by the electron recombination time, is sufficient to exert a torque on magnetization. The spin lifetime of holes is dominated by the strong SOC and it is estimated to be ~ 1 - 10 fs [84] which is not enough to cause the OSTT [21], so we will omit holes in further discussion.

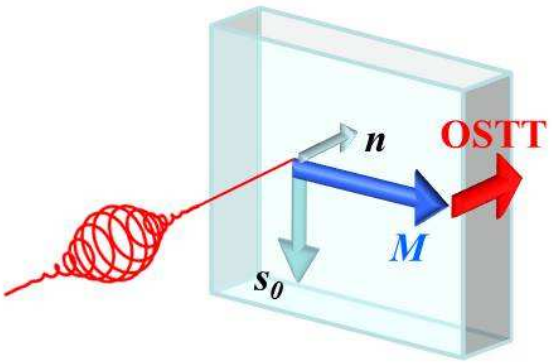

Fig. 10: Schematic illustration of the optical spin transfer torque. The circularly polarized light generates the carrier spin polarization, where the initial orientation of spins (***n***) is parallel with the incident light direction and perpendicular to magnetization (***M***). The steady-state component of the injected spin density ($\boldsymbol{s_0}$) is oriented in the sample plane, perpendicular to ***M***, and exerts a torque on the magnetization vector ***M***.

Right after the impact of the circularly polarized light, the orientation of the generated spins (***n***) is given by the propagation direction and by helicity of the circular polarization. However, the exchange field produced by the Mn moment yields the electron spins precession around the magnetization vector (***M***), with the precessing period ~ 100 fs [84]. As the electron spin lifetime highly exceeds this precession period, the spins precess many times before they relax. In this regime, the steady-state spin density ($\boldsymbol{s_0}$) is oriented in the plane of the sample, but perpendicular to ***M***, and exerts a torque on the magnetization vector, which leads to the subsequent precession of magnetization. It is important to note, that the OSTT starts to act during the laser pulse impact (when the electrons with a concentration δn_e are photoinjected) and fades away within the electron spin lifetime (~ picoseconds). However, the magnetization precession persists up to several nanoseconds. The influence of OSTT is, therefore, most clearly observable in the initial phase of the detected MO signal, see Ref. 21 in Appendix 6 for the measured magnetization trajectories.

6. Determination of micromagnetic parameters

The magnetic properties of any ferromagnetic material are described by the micromagnetic parameters, such as the magnetic anisotropy constants, spin stiffness or the Gilbert damping parameter. There are many different experimental methods that have been developed in order to measure these micromagnetic parameters. In particular, the ferromagnetic resonance (FMR), SQUID magnetometry or the magneto-transport measurements belong among the most commonly used ones [46, 47, 86]. However, it was shown recently by Němec et *al*. [33] (see Appendix 8) that the time-resolved MO spectroscopy can be also exploited in the investigation of the mentioned micromagnetic parameters of the ferromagnet. Moreover, this technique can overcome some of the limitations (e.g., the spatial resolution, the separation of the inhomogeneous contribution to the resonance linewidth, …) of the other experimental techniques [33, 82]. The aim of this chapter is to demonstrate the ability of this powerful technique to deduce all the micromagnetic parameters from a *single* MO pump-and-probe experiment.

Before proceeding to the determination of the anisotropy constants K_i, the Gilbert damping parameter α and the spin stiffness constant D, the analytical description of magnetization dynamics has to be performed as it forms the basis of the whole experimental method. The magnetization dynamics after the impact of the laser pulse can by described by the Landau-Lifshitz-Gilbert (LLG) equation:

$$\frac{d\boldsymbol{M}(t)}{dt} = -\gamma\left[\boldsymbol{M}(t) \times \boldsymbol{H_{eff}}(t)\right] + \frac{\alpha}{M_s}\left[\boldsymbol{M}(t) \times \frac{d\boldsymbol{M}(t)}{dt}\right], \tag{16}$$

where $\gamma = (g\mu_B)/\hbar$ is the gyromagnetic ratio with Landé g-factor $g = 2$ and Bohr magneton μ_B, $\boldsymbol{H_{eff}}$ is the effective magnetic field, α is the Gilbert damping constant and M_s is the saturated magnetization. Since the MO spectroscopy is sensitive both to the in-plane and out-of-plane positions of magnetization, it is convenient to rewrite the LLG equation into the spherical coordinates, characterized by the polar θ and azimuthal φ angles, respectively [43]:

$$\frac{dM_s}{dt} = 0, \tag{17}$$

$$\frac{d\theta}{dt} = -\frac{\gamma}{(1+\alpha^2)M_s}\left(\alpha \cdot A + \frac{B}{sin\theta}\right), \tag{18}$$

$$\frac{d\varphi}{dt} = -\frac{\gamma}{(1+\alpha^2)M_s sin\theta}\left(A - \frac{\alpha \cdot B}{sin\theta}\right), \tag{19}$$

where $A = dF/d\theta$ and $B = dF/d\varphi$ are the derivatives of the free energy functional F (see Eq. 1 in Chap. 2.3) with respect to θ and φ, respectively. For small deviations $\delta\theta$ and $\delta\varphi$ from their equilibrium values θ_0 and φ_0, the solution of Eqs. 18 and 19 can be written in the form $\theta(t) = \theta_0 + \delta\theta(t)$ and $\varphi(t) = \varphi_0 + \delta\varphi(t)$ as [Supplementary in 33, 43]:

$$\theta(t) = \theta_0 + A_\theta e^{-t/t_G} cos(2\pi f t + \Phi_\theta), \tag{20}$$

$$\varphi(t) = \varphi_0 + A_\varphi e^{-t/t_G} cos\big(2\pi f t + \Phi_\varphi\big), \tag{21}$$

where the constants A_θ (A_φ) and Φ_θ (Φ_φ) describe the initial amplitude and phase of θ (φ), respectively. For the typical geometry for the pump-and-probe experiment in (Ga,Mn)As with the in-plane position of magnetization (θ_0 = 90˚) and the external magnetic field applied also in-plane (θ_H = 90˚), the precession frequency and the damping time are given (assuming the relatively slow precession damping; α^2 = 0) [Supplementary in 33]:

$$f = \frac{g\mu_B}{h}\sqrt{\begin{matrix}\left[H_{ext}cos(\varphi-\varphi_H) - 2K_{out} + \frac{K_C(3+\cos 4\varphi)}{2} + 2K_u sin^2\left(\varphi - \frac{\pi}{4}\right)\right]\times \\ \times\left[H_{ext}cos(\varphi-\varphi_H) + 2K_c cos4\varphi - 2K_u sin2\varphi\right]\end{matrix}}, \tag{22}$$

$$\frac{1}{t_G} = \alpha\frac{g\mu_B}{2\hbar}\left(2H_{ext}cos(\varphi-\varphi_H) - 2K_{out} + \frac{K_c}{2}(3+5cos4\varphi) + K_u(1-3sin2\varphi)\right). \tag{23}$$

As seen from Eq. 22, the magnetization oscillation frequency reflects the sensitivity to the magnetic anisotropy of the material (described by the magnetic anisotropy constants K_i). This well-known fact is the basic principle of the FMR technique [47, 48] and will be also exploited in the time-resolved MO method (see Chap. 6.1). Equation 23 shows that the Gilbert damping time, which is measured experimentally (see Chap. 4.1), depends not only on the Gilbert damping parameter α, but also on the anisotropy constants and the mutual orientation of the external magnetic field and the magnetization. We note that the dependence of α on K_i was omitted in the previous publications [76, 77, 78] which may be the reason of the large scatter in the reported values of α.

6.1 Magnetic anisotropy constants

The dependence of the oscillation frequency on the magnetic anisotropy and on the external magnetic field magnitude and orientation enables the direct calculation of the anisotropy constants K_i from the measured time-resolved MO signal. In particular, for a sufficiently strong magnetic field, which aligns the magnetization into its direction (i.e., $\varphi = \varphi_H$), the following equations can be used to fit the obtained precession frequencies:

$$f = \frac{g\mu_B}{h}\sqrt{(H_{ext} - 2K_{out} + K_c)(H_{ext} - 2K_c - 2K_u)} \tag{24}$$

for H_{ext} along the [110] crystallographic direction (i.e. $\varphi_H = \pi/4$), or

$$f = \frac{g\mu_B}{h}\sqrt{(H_{ext} - 2K_{out} + 2K_c + K_u)(H_{ext} + 2K_c)} \tag{25}$$

for H_{ext} along the [010] crystallographic direction (i.e. $\varphi_H = \pi/2$), or

$$f = \frac{g\mu_B}{h}\sqrt{(H_{ext} - 2K_{out} + K_c + 2K_u)(H_{ext} - 2K_c + 2K_u)} \tag{26}$$

for H_{ext} along the [-110] crystallographic direction (i.e. $\varphi_H = 3\pi/4$).

In principle, only three precession frequencies in one magnetic field orientation are needed to obtain all three anisotropy constants K_c, K_u and K_{out}. However, the precision of the magnetic anisotropy determination can be increased when measuring the $f(H_{ext})$ dependence for at least two different orientations of H_{ext} as shown in Fig. 11a.

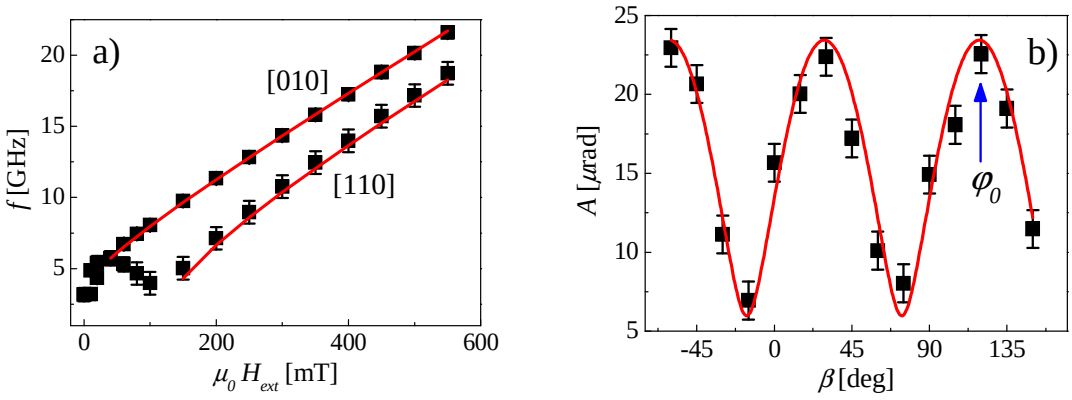

Fig. 11: a) Dependence of the magnetization precession frequency f on the external magnetic field H_{ext} applied along the [010] and [110] crystallographic directions; the red lines are the fits by Eqs. 24 and 25, respectively, with K_c = 31 mT, K_u = 27.5 mT and K_{out} = -190 mT. b) Probe polarization dependence of the oscillatory amplitude A obtained by fitting the measured MO signals by Eq. 7. The red line is the fit by Eq. 10 and the blue vertical arrow depicts the obtained equilibrium easy axis position $\varphi_0 \approx 120^\circ$. The measurements were performed in (Ga,Mn)As sample with 5.2% Mn concentration at the base temperature of 15 K.

The precision can be increased even further when the EA position of magnetization is known. In (Ga,Mn)As samples with the in-plane magnetization orientation, the position of the EA is given by the relative magnitude of K_c and K_u and, therefore, the knowledge of the EA position enables the direct determination of the ratio K_c/K_u. As mention in Chap. 4.2.2, the equilibrium position of the EA can be determined from the amplitude of the time-resolved MO signals when the magnetization dynamics are measured for the different orientations of the linearly polarized probe pulses β, see Fig. 11b.

6.2 Gilbert damping parameter α

The Gilbert damping constant α can be obtained from the numerical modeling of the measured MO data. In the first step, the time-dependent deviations of the spherical angles $[\delta\theta(t), \delta\varphi(t)]$ from their equilibrium values θ_0 and φ_0 are computed by the LLG equation (Eqs. 18 and 19), using the determined anisotropy constants K_i. In the second step it is calculated how such changes of θ and φ modify the static MO response of the sample MO^{stat}, which is the measured signal represented by Eq. 12 in Chap. 4.2.3. The data can be reliably modeled from the time delays ~ 100 ps when the quasi-equilibrium precession of magnetization is established. The only parameters in this modeling procedure are the Gilbert damping coefficient α, the initial deviation of the spherical angles from the corresponding equilibrium positions and the parameters describing the in-plane movement of the easy axis and the

demagnetization signal, which are apparent as the non-oscillatory signal in the measured magnetization dynamics (see Eq. 2 in Chap. 4.1). We note that the magnitude of the initial deviation of the spherical angles, calculated in the model, is strongly dependent on the input value of the static MO coefficients P^{PKE} and P^{MLD}. However, the values of the MO coefficients, which are always measured with some precision, has no influence on the determined value of α. Applying this modeling procedure, the dependence of α on the external magnetic field H_{ext} or on the oscillation frequency f can be obtained, respectively (see Fig. 4 in Appendix 8).

In contrast to the theoretical predictions that α does not depend on the oscillation frequency [87], we observed experimentally that in (Ga,Mn)As α decreases monotonously with increasing oscillation frequency [33] and saturates for $f > 15$ GHz [33], which is in accord with the results reported for other ferromagnetic materials [88, 89]. The most probable explanation of this effect was given by Walowski *et al.* in Ref. 88, where it was assumed that in the low field range (low precession frequency) the small magnetization inhomogeneities can be build, meaning that the magnetization is not fully aligned with H_{ext} but forms ripples. Consequently, the measured MO signal, which detects sample properties averaged over the laser spot size, experiences apparent oscillation damping α, because the magnetic properties (i.e. the precession frequencies) are slightly different within the spot size. On the other hand, for stronger external fields the sample is fully homogeneous and, therefore, the precession damping is not dependent on the applied field. It was found that for (Ga,Mn)As samples the frequency-independent Gilbert damping is strongly dependent on the Mn concentration and it decreases systematically from 0.1 to 0.01 when the nominal Mn concentration increases from 2% to 9% [33] (see Fig. 4b in Appendix 8).

6.3 Spin stiffness

The spin stiffness, which describes the exchange energy associated with the twist of the spins, is one of the most important material parameters that characterize the magnetic properties of a ferromagnet. So far, the spin stiffness in (Ga,Mn)As was typically obtained from the measurements of the spin precession modes by the FMR technique [90, 91]. The precession modes represent the spin wave resonances (SWRs, also known as magnons) that are selectively amplified by fulfilling the boundary conditions of the thin FM film (see e.g. Ref. 43 for detailed discussion). In FMR the SWRs are investigated in the frequency-domain, where they manifest as the multiple absorption peaks in the spectra. However, the SWRs can be also studied in the time-domain by the time-resolved MO spectroscopy [33, 92], where they are apparent as the additional frequencies (f_n) that are larger than that of the uniform magnetization precession (f_0), see Fig. 5 in Appendix 8. For the external magnetic field H_{ext} applied in the sample plane, the angular frequency of the n-th SWR mode f_n is given [33, 92]:

$$f_n = \frac{g\mu_B}{h}\sqrt{\begin{matrix}\left[H_{ext}cos(\varphi-\varphi_H) - 2K_{out} + \frac{K_C(3+\cos 4\varphi)}{2} + 2K_u sin^2\left(\varphi-\frac{\pi}{4}\right)\right]\times \\ \times\left[H_{ext}cos(\varphi-\varphi_H) + 2K_c cos4\varphi - 2K_u sin2\varphi\ +\ \Delta H_n\right]\end{matrix}}, \qquad (27)$$

where $\Delta H_n = H_0 - H_n$ is the shift of the resonant field for the higher index n spin wave modes with respect to the uniform precession mode $n = 0$. For the magnetically homogeneous films, the value of ΔH_n is given by the Kittel relation [90]:

$$\Delta H_n = H_0 - H_n = n^2 \frac{D}{g\mu_B} \frac{\pi^2}{L^2}, \tag{28}$$

where D is the exchange spin stiffness constant, μ_B is the Bohr magneton, g is the Lande g-factor and L is the thickness of the magnetic film. This equation is of high importance as it enables an evaluation of the spin stiffness D from the field differences ΔH_n that can be obtained from the measured frequency spacing of the individual modes (see Eq. 27). It is important to emphasize that Eq. 28 is only valid for the magnetically homogenous films, i.e. for films where the (Ga,Mn)As layer thickness does not exceed ~ 50 nm [32, 33, 43].

Let's now proceed to the exact procedure how the spin stiffness parameter D can be obtained from the time-resolved MO signal. For this purpose, the detection of *at least* one additional SWR, together with the uniform precessional mode $n = 0$, is inevitable, but the more SWRs are detected the more precise determination of D can be performed. We note that multiple SWRs can be observed in thick (Ga,Mn)As samples ($L \geq 50$ nm) [43, 90], but not all of them could be ascribed to Kittel modes, most probably because of the magnetic inhomogeneity of the magnetic layer [43]. Consequently, it is a rather delicate task to evaluate the value of D because the measurement has to be performed on a thick enough film to observe a multiple SWRs but thin enough to prevent its magnetic inhomogeneity. In magnetically homogeneous (Ga,Mn)As samples ($L \leq 50$ nm) we observed three SWRs at most [33, 43]. We note that the most precise procedure how the precession frequencies f_n can be evaluated from the measured MO data is from the Fourier spectra of the oscillatory part of the MO signals. The values H_n can be obtained from the measured dependencies $f_n(H_{ext})$ - for a sufficiently high H_{ext}, the equilibrium position of the EA is aligned with H_{ext} (i.e., $\varphi = \varphi_H$) and the measured $f_n(H_{ext})$ dependencies can be fitted by Eq. 27 for each n, obtaining the only unknown parameter ΔH_n. Finally, the spin stiffness coefficient D can be determined from Eq. 28.

We used this method in the optimized set of (Ga,Mn)As samples and we observed that the spin stiffness parameter D is a weakly increasing function of the Mn doping, with the values of D between 2 and 3 meVnm^2 for the studied samples with the nominal Mn doping from 3.8% to 9%, see Ref. 33 in Appendix 8, where all the results are summarized.

CONCLUSIONS

The ferromagnetic semiconductor (Ga,Mn)As is a very interesting material for the spintronics. Not only it is a material where the proof-of-concept spintronic devices can be realized, but it is also a good model material where new physical phenomena can be discovered and thoroughly studied, and the gained knowledge can be subsequently transferred to conventional room-temperature ferromagnetic metals. The aim of this doctoral thesis was to investigate the magnetic properties of (Ga,Mn)As. We focused mainly on the magnetization dynamics induced by the impact of the ultrashort laser pulses, because the ultrafast manipulation with the magnetic order is of high importance for future envisioned spintronic devices.

We studied an extensive set of high quality (Ga,Mn)As samples with Mn doping ranging from 1.5% to 14%. Using the time-resolved magneto-optical (MO) spectroscopy we observed the laser-induced precession of magnetization in all the samples, except in those with the lowest and the highest Mn concentration, where the magnetic anisotropy was too strong to be significantly influenced by the impact of the laser pulse. We used the magnetic anisotropy-related precession of magnetization as a spectroscopic method for evaluation of all the basic micromagnetic parameters of (Ga,Mn)As – the magnetic anisotropy constants, the Gilbert damping coefficient, and the spin stiffness – from one single set of experimental data. We found a clear monotonous dependence of these parameters on Mn doping, i.e., on the hole concentration and magnetization magnitude, which can be of practical use in the material property engineering.

Moreover, the detailed analysis of the measured MO signals enabled us to establish a new experimental method that can be used for a determination of the real-space magnetization trajectory without any numerical modeling. This real-space magnetization dynamics contributed significantly to our understanding of the mechanism of the laser-induced magnetization dynamics. In particular, we revealed that it can be either of thermal or of non-thermal origin, depending on the light intensity and polarization state. The understanding of these mechanisms enabled us to identify two new physical phenomena – the optical spin transfer torque and the optical spin-orbit torque, which were theoretically predicted but so far experimentally unobserved. Both these effects can have a large impact on the basic research towards the development of the future spintronic applications because they act on a timescale that is several orders of magnitude shorter than in the case of their current-induced counterparts.

BIBLIOGRAPHY

[1] W. M. Chen, I. A. Buyanova: *Handbook of Spintronic Semiconductors*. Pan Stanford Publishing (2010).

[2] D. Awschalom, M. F. Flatté: *Challenges for semiconductor spintronics*. Nat. Phys. **3**, 153 (2007).

[3] I. Žutić, J. Fabian, S. Das Sarma: *Spintronics: Fundamentals and Applications.* Rev. Mod. Phys. **76,** 323 (2004).

[4] Editorial: *More than just room temperature*. Nat. Mater. **9**, 951 (2010).

[5] A.V. Kimel, G.V. Astakhov, A. Kirilyuk, G. M. Schott, G. Karczewski, W. Ossau, G. Schmidt, L.W. Molenkamp, Th. Rasing: *Observation of Giant Magnetic Linear Dichroism in (Ga,Mn)As.* Phys. Rev. Lett. **94**, 227203 (2005).

[6] H. Ohno: *Making Nonmagnetic Semiconductors Ferromagnetic*. Science **281**, 951 (1998).

[7] J. K. Furdyna: *Diluted magnetic semiconductors*. J. Appl. Phys. **64**, R29 (1988).

[8] V. Novák, K. Olejník, J. Wunderlich, M. Cukr, K. Výborný, A. W. Rushforth, K. W. Edmonds, R. P. Campion, B. L. Gallagher, J. Sinova, T. Jungwirth: *Curie point singularity in the temperature derivative of resistivity in (Ga,Mn)As*. Phys. Rev. Lett. **101**, 077201 (2008).

[9] M. Wang, R. P. Campion, A. W. Rushforth, K. W. Edmonds, C. T. Foxon, B. L. Gallagher: *Achieving high Curie temperature in (Ga,Mn)As*. Appl. Phys. Lett. **93**, 132103 (2008).

[10] H. Ohno: *A window on the future of spintronics*. Nat. Mater. **9**, 952 (2010).

[11] H. Ohno, D. Chiba, F. Matsukura, T. Omiya, E. Abe, T. Dietl, Y. Ohno, K. Ohtani: *Electric-field control of ferromagnetism*. Nature **408**, 944 (2000).

[12] N. Samarth: *A model ferromagnetic semiconductor*. Nat. Mater. **9**, 955 (2010).

[13] M. Tanaka, Y. Higo: *Large Tunneling Magnetoresistance in GaMnAs/AlAs/GaMnAs Ferromagnetic Semiconductor Tunnel Junctions*. Phys. Rev. Lett. **87**, 026602 (2001).

[14] H. Saito, S. Yuasa, K. Ando: *Origin of the Tunnel Anisotropic Magnetoresistance in* $Ga_{1-x}Mn_xAs/ZnSe/Ga_{1-x}Mn_xAs$ *Magnetic Tunnel Junction of II-VI/III-V Heterostructures*. Phys. Rev. Lett. **95**, 086604 (2005).

[15] J. Sinova, I. Žutić: *New moves of the spintronics tango*. Mat. Matter. **11**, 368 (2012).

[16] C. Gould, C. Ruster, T. Jungwirth, E. Girgis, G. M. Schott, R. Giraud, K. Brunner, G. Schmidt, L. W. Molenkamp: *Tunneling Anisotropic Magnetoresistance: A Spin-Valve-Like Tunnel Magnetoresistance Using a Single Magnetic Layer*. Phys. Rev. Lett. **93**, 117203 (2004).

[17] B. G. Park, J. Wunderlich, X. Martí, V. Holý, Y. Kurosaki, M. Yamada, H. Yamamoto, A. Nishide, J. Hayakawa, H. Takahashi, A. B. Shick, T. Jungwirth: *A spin-valve-like magnetoresistance of an antiferromagnet-based tunnel junction*. Nat. Matter. **10**, 347 (2011).

[18] J. Wunderlich, T. Jungwirth, B. Kaestner, A. C. Irvine, A. B. Shick, N. Stone, K.-Y. Wang, U. Rana, A. D. Giddings, C. T. Foxon, R. P. Campion, D. A. Williams, B. L. Gallagher: *Coulomb Blockade Anisotropic magnetoresistance Effect in a (Ga,Mn)As Single-Electron Transistor*. Phys. Rev. Lett. **97**, 077201 (2006).

[19] S. Mark, P. Durrenfeld, K. Pappert, L. Ebel, K. Brunner, C. Gould, L. W. Molenkamp: *Fully Electrical Read-Write Device Out of a Ferromagnetic Semiconductor*. Phys. Rev. Lett. **106**, 057204 (2011).

[20] D. C. Ralpha, M. D. Stiles: *Spin transfer torques*. J. Magn. Magn. Matter. **320**, 1190 (2008).

[21] P. Němec, E. Rozkotová, N. Tesařová, F. Trojánek, E. De Ranieri, K. Olejník, J. Zemen, V. Novák, M. Cukr, P. Malý, T. Jungwirth: *Experimental observation of the optical spin transfer torque*. Nat. Phys. **8**, 411 (2012).

[22] A. Brataas, A. D. Kent, H. Ohno*: Current-induced torques in magnetic materials*. Nat. Matter. **11**, 372 (2012).

[23] A. Chernyshov, M. Overby, Y. Lyanda-Geller, L. P. Rokhinson: *Evidence for reversible control of magnetization in a ferromagnetic material via spin-orbit magnetic field*. Nat. Phys. **5**, 656 (2009).

[24] N. Tesařová, P. Němec, E. Rozkotová, J. Zemen, T. Janda, D. Butkovičová, F. Trojánek, K. Olejník, V. Novák, P. Malý, T. Jungwirth: *Experimental observation of the optical spin-orbit torque*. Submitted to Nature Photonics, arXiv: 1207.0307.

[25] T. Dietl, H. Ohno, F. Matsukura, J. Cibert, D. Ferrand: *Zener Model Description of Ferromagnetism in Zinc-Blende Magnetic Semiconductors*. Science **287**, 1019 (2000).

[26] M. Dobrowolska, K. Tivakornsasithorn, X. Liu, J. K. Furdyna, M. Berciu, K. M. Yu, W.Walukiewicz: *Controlling the Curie temperature in (Ga,Mn)As through location of the Fermi level within the impurity band*. Nat. Matter. **11**, 444 (2012).

[27] T. Jungwirth, J. Sinova, A. H. MacDonald, B. L. Gallagher, V. Novák, K. W. Edmonds, A. W. Rushforth, R. P. Campion, C. T. Foxon, L. Eaves, E. Olejník, J. Mašek, S.-R. Eric Yang, J. Wunderlich, C. Gould, L. W. Molenkamp, T. Dietl, H. Ohno: *Character of states near the Fermi level in (Ga,Mn)As: Impurity to valence band crossover*. Phys. Rev. B **76**, 125206 (2007).

[28] T. Jungwirth, J. Sinova, J. Mašek, J. Kučera, A. H. MacDonald: *Theory of ferromagnetic III-V semiconductors.* Rev. Mod. Phys. **78,** 809 (2006).

[29] T. Jungwirth, K. Y. Wang, J. Mašek, K. W. Edmonds, J. König, J. Sinova, M. Polini, N. A. Goncharuk, A. H. MacDonald, M. Sawicki, A. W. Rushforth, R. P. Campion, L. X. Zhao, C. T. Foxon, B. L. Gallagher: *Prospects for high temperature ferromagnetism in (Ga,Mn)As semiconductors*. Phys. Rev. B **72**, 165204 (2005).

[30] Th. Hartmann, S. Ye, P. J. Klar, W. Heimbrodt, M. Lampalzer, W. Stolz, T. Kurz, A. Loidl, H.-A. Krug von Nidda, D. Wolverson, J. J. Davies, H. Overhof: *Tuning of the average p-d exchange in (Ga,Mn)As by modification of the Mn electronic structure*. Phys. Rev. B **70**, 233201 (2004).

[31] K. S. Burch, D. D. Awschalom, D. N. Basov: *Optical properties of III-Mn-V ferromagnetic semiconductors*. J. Magn. Magn. Matter. **320**, 3207 (2008).

[32] T. Jungwirth, P. Horodyská, N. Tesařová, P. Němec, J. Šubrt, P. Malý, P. Kužel, C. Kadlec, J. Mašek, I. Němec, M. Orlita, V. Novák,1 K. Olejník, Z. Šrobáň , P. Vašek, P. Svoboda, J. Sinova: *Systematic Study of Mn-Doping Trends in Optical Properties of (Ga,Mn)As*. Phys. Rev. Lett. **105**, 227201 (2010).

[33] P. Němec, V. Novák, N. Tesařová, E. Rozkotová, H. Reichlová, D. Butkovičová, F. Trojánek, K. Olejník, P. Malý, R. P. Campion, B. I. Gallagher, J. Sinova, T. Jungwirth: *Establishing micromagnetic parameters of ferromagnetic semiconductor (Ga,Mn)As*. Accepted in Nature Communications, arXiv: 1207.0310.

[34] M. I. Dyakonov: *Spin physics in semiconductors.* Springer-Verlag, Berlin - Heidelberg, 2009.

[35] P. Y. Yu, M. Cardona: *Fundametals of Semiconductors*, Springer (1996).

[36] J. Mašek, F. Máca, J. Kudrnovský, O. Makarovsky, L. Eaves, R. P. Campion, K.W. Edmonds, A.W. Rushforth, C. T. Foxon, B. L. Gallagher, V. Novák, J. Sinova, T. Jungwirth: *Microscopic Analysis of the Valence Band and Impurity Band Theories of (Ga,Mn)As*. Phys. Rev. Lett. **105**, 227202 (2010).

[37] K. Ando, H. Saito, K. C. Agarwal, M. C. Debnath, V. Zayets: *Origin of the Anomalous Magnetic Circular Dichroism Spectral Shape in Ferromagnetic $Ga_{1-x}Mn_xAs$: Impurity Bands inside the Band Gap*. Phys. Rev. Lett. **100**, 067204 (2008).

[38] K. S. Burch, D. B. Shrekenhamer, E. J. Singley, J. Stephens, B. L. Sheu, R. K. Kawakami, P. Schiffer, N. Samarth, D. D. Awschalom, D. N. Basov: *Impurity Band Conduction in a High Temperature Ferromagnetic Semiconductor*. Phys. Rev. Lett. **97**, 087208 (2006).

[39] M. J. Tang, M. E. Flatté: *Magnetic Circular Dichroism from the Impurity Band in III-V Diluted Magnetic Semiconductors*. Phys. Rev. Lett. **101**, 157203 (2008).

[40] S. Ohya, K. Takata, M. Tanaka: *Nearly non-magnetic valence band of the ferromagnetic semiconductor GaMnAs*. Nat. Phys. **7**, 342 (2011).

[41] J. Zemen, J. Kučera, K. Olejník, T. Jungwirth: *Magnetocrystalline anisotropies in (Ga,Mn)As: Systematic theoretical study and comparison with experiment.* Phys. Rev. B **80,** 155203 (2009).

[42] M. Birowska, C. Śliwa, J. A. Majewski, T. Dietl: *Origin of bulk uniaxial anisotropy in zinc-blende dilute magnetic semiconductors*. Phys. Rev. Lett. **108**, 237203 (2012).

[43] E. Schmorazerová: *Spin dynamics in GaAs-based semiconductor structures.* Doctoral thesis, Charles University in Prague, Prague (2012).

[44] M. Abolfath, T. Jungwirth, J. Brum, A. H. MacDonald: *Theory of magnetic anisotropy in $III_{1-x}Mn_xV$ ferromagnets*. Phys. Rev. B **63**, 054418 (2001).

[45] K. Hamaya, T. Watanabe, T. Taniyama, A. Oiwa, Y. Kitamoto, Y. Yamazaki: *Magnetic anisotropy switching in (Ga,Mn)As with increasing hole concentration*. Phys. Rev. B **74**, 045201 (2006).

[46] K. Olejník: *Preparation and characterization of ferromagnetic GaMnAs epilayers.* Doctoral thesis, Charles University in Prague, Prague (2009).

[47] X. Liu, J. K. Furdyna: *Ferromagnetic resonance in $Ga_{1-x}Mn_xAs$ dilute magnetic semiconductors*. J. Phys.: Condens. Matter **18**, R245 (2006).

[48] K. Khazen: *Ferromagnetic Resonance Investigation of GaMnAs Nanometric Layers.* Doctoral thesis, Université Paris VI - Pierre et Marie Curie Institut des NanoSiences de Paris, Paris (2008).

[49] C. S. King, J. Zemen, K. Olejník, L. Horák, J. A. Haigh, V. Novák, A. Irvine, J. Kučera, V. Holý: *Strain control of magnetic anisotropy in (Ga,Mn)As microbars*. Phys. Rev. B **83**, 115312 (2011).

[50] B. Beschoten, P. A. Crowell, I. Malajovich, D. D. Awschalom: *Magnetic Circular Dichroism Studies of Carrier-Induced Ferromagnetism in $(Ga_{1-x}Mn_x)As$*. Phys. Rev. Lett. **83**, 3073 (1999).

[51] T. Kuroiwa, T. Yasuda, F. Matsukura, A. Shen, Y. Ohno, Y. Segawa, H. Ohno: *Faraday rotation of ferromagnetic (Ga, Mn)As*. Electron. Lett. **34**, 190 (1998).

[52] A.V. Kimel, G.V. Astakhov, A. Kirilyuk, G. M. Schott, G. Karczewski, W. Ossau, G. Schmidt, L.W. Molenkamp, Th. Rasing: *Observation of Giant Magnetic Linear Dichroism in (Ga,Mn)As*. Phys. Rev. Lett. **94**, 1227203 (2005).

[53] G. Acbas, M.-H. Kim, M. Cukr, V. Novák, M. A. Scarpulla, O. D. Dubon, T. Jungwirth, J. Sinova, J. Cerne: *Electronic Structure of Ferromagnetic Semiconductor $Ga_{1-x}Mn_xAs$ Probed by Subgap Magneto-optical Spectroscopy*. Phys. Rev. Lett. **103**, 137201 (2009).

[54] A. K. Zvezdin, V. A. Kotov: *Moderen Magnetooptics and Magnetooptical Materials.* Institute of Physics, Bristol, Philadelphia (1997).

[55] K. Postava, J. Pištora: *Magneto-optical effects in thin films*. Sborník vědeckých prací Vysoké školy báňské – Technické Univerzity Ostrava, číslo 1, ročník XLV (1999).

[56] R. Lang, A. Winter, H. Pascher, H. Krenn, X. Liu, J. K. Furdyna: *Polar Kerr effect studies of $Ga_{1-x}Mn_xAs$ epitaxial films*. Phys. Rev. B **72**, 024430 (2005).

[57] D. Hrabovsky, E. Vanelle, A. R. Fert, D. S. Yee, J. P. Redoules, J. Sadowski, J. Kanski, L. Ilver: *Magnetization reversal in GaMnAs layers studied by Kerr effect*. Appl. Phys. Lett. **81**, 2806 (2002).

[58] M.-H. Kim, G. Acbas, M.-H. Yang, M. Eginligil, P. Khalifah, I. Ohkubo, H. Christen, D. Mandrus, Z. Fang, J. Cerne: *Infrared anomalous Hall effect in SrRuO3: Exploring evidence for crossover to intrinsic behavior*. Phys. Rev. B **81**, 235218 (2010).

[59] E. Rozkotová, P. Němec, P. Horodyská, D. Sprinzl, F. Trojánek, P. Malý, V. Novák, K. Olejník, M. Cukr, T. Jungwirth: *Light-induced magnetization precession in GaMnAs*. Appl. Phys. Lett. **92**, 122507 (2008).

[60] E. Rozkotová, P. Němec, N. Tesařová, P. Malý, V. Novák, K. Olejník, M. Cukr, T. Jungwirth: *Coherent control of magnetization precession in ferromagnetic semiconductor (Ga,Mn)As*. Appl. Phys. Lett. **93**, 232505 (2008).

[61] J. Qi, Y. Xu, A. Steigerwald, X. Liu, J. K. Furdyna, I. E. Perakis, N. H. Tolk: *Ultrafast laser-induced coherent spin dynamics in ferromagnetic $Ga_{1-x}Mn_xAs/GaAs$ structures*. Phys. Rev. B **79**, 085304 (2009).

[62] R. M. Osgood, S. D. Bader, B. M. Clemens, R. L. White, H. Matsuyama: *Second-order magneto-optic effects in anisotropic thin films*. J. Magn. Magn. Mater. **182**, 297 (1998).

[63] K. Postava, H. Jaffres, A. Schuh, F. Nguyen Van Dau, M. Goiran, A.R. Fert: *Linear and quadratic magneto-optical measurements of the spin reorientation in epitaxial Fe films on MgO*. J. Magn. Magn. Mater. **172**, 199 (1997).

[64] G. P. Moore, J. Ferré, A. Mougin, M. Moreno, L. Daweritz: *Magnetic anisotropy and switching process in diluted $Ga_{1-x}Mn_xAs$ magnetic semiconductor films*. J. Appl. Phys. **94**, 4530 (2003).

[65] N. Tesařová, J. Šubrt, P. Malý, P. Němec, C. T. Ellis, A. Mukherjee, J. Cerne: *High Precision Magnetic Linear Dichroism Measurements in (Ga,Mn)As*. Accepted in Rev. Sci. Intrum., arXiv: 1212.0956.

[66] N. Tesařová, P. Němec, E. Rozkotová, J. Šubrt, H. Reichlová, D. Butkovičová, F. Trojánek, P. Malý, V. Novák, T. Jungwirth: *Direct measurement of the three-dimensional magnetization vector trajectory in GaMnAs by a magneto-optical pump-and-probe method*. Appl. Phys. Lett. **100**, 102403 (2012).

[67] E. De Ranieri, A. W. Rushforth, K. Výborný, U. Rana, E. Ahmad, R. P. Campion, C. T. Foxon, B. L. Gallagher, A. C. Irvine, J. Wunderlich, T. Jungwirth: *Lithographically and electrically controlled strain effects on anisotropic magnetoresistance in (Ga,Mn)As*. New J. Phys. **10**, 065003 (2008).

[68] B. Al-Qadi, N. Nishizawa, K. Nishibayashi, M. Kaneko, H. Munekata: *Thickness dependence of magneto-optical effects in (Ga,Mn)As epitaxial layers*. Appl. Phys. Lett. **100**, 222410 (2012).

[69] A. Kirilyuk, A.V. Kimel, T. Rasing: *Ultrafast optical manipulation of magnetic order*. Rev. Mod. Phys. **80**, 2731 (2010).

[70] G. E. Rowlands, T. Rahman, J. A. Katine, J. Langer, A. Lyle, H. Zhao, J. G. Alzate, A. A. Kovalev, Y. Tserkovnyak, Z. M. Zeng, H. W. Jiang, K. Galatsis, Y. M. Huai, P. Khalili Amiri, K. L. Wang, I. N. Krivorotov, J.-P. Wang: *Deep subnanosecond spin torque switching in magnetic tunnel junctions with combined in-plane and perpendicular polarizers*. Appl. Phys. Lett. **98**, 102509 (2011).

[71] E. Beaurepaire, J.-C. Merle, A. Daunois, J.-Y. Bigot: *Ultrafast Spin Dynamics in Ferromagnetic Nickel*. Phys. Rev. Lett. **76**, 4250 (1996).

[72] J. Wang, Ch. Sun, Y. Hashimoto, J. Kono, G. A. Khodaparast, L. Cywinski, L. J. Sham, G. D. Sanders, Ch. J. Stanton, H. Munekata: *Ultrafast magneto-optics in ferromagnetic III–V semiconductors*. J. Phys. Cond. Matt. **18**, R501 (2006).

[73] E. Kojima, R. Shimano, Y. Hashimoto, S. Katsumoto, Y. Iye, M. Kuwata-Gonokami: *Observation of the spin-charge thermal isolation of ferromagnetic $Ga_{0.94}Mn_{0.06}As$ by time-resolved magneto-optical measurements*. Phys. Rev. B **68**, 193203 (2003).

[74] A. Oiwa, H. Takechi, H. Munekata: *Photoinduced magnetization rotation and precessional motion of magnetization in ferromagnetic (Ga,Mn)As.* J. Supercond. **19**, 9 (2005).

[75] J. Wang, I. Cotoros, K. M. Dani, X. Liu, J. K. Furdyna, D. S. Chemla: *Ultrafast Enhancement of Ferromagnetism via Photoexcited Holes in GaMnAs.* Phys. Rev. Lett. **98**, 217401 (2007).

[76] J. Qi, Y. Xu, N. H. Tolk, X. Liu, J. K. Furdyna, I. E. Perakis*: Coherent magnetization precession in GaMnAs induced by ultrafast optical excitation*. Appl. Phys. Lett. **91**, 112506 (2007).

[77] Y. Hashimoto, S. Kobayashi, H. Munekata: *Photoinduced precession of magnetization in ferromagnetic (Ga,Mn)As*. Phys. Rev. Lett. **100,** 067202 (2008).

[78] S. Kobayashi, Y. Hashimoto, H. Munekata: *Investigation of an eff ective anisotropy field involved in photoinduced precession of magnetization in (Ga,Mn)As.* J. Appl. Phys. **105**, 07C519 (2009).

[79] N. Tesařová, P. Němec, E. Rozkotová, F. Trojánek, P. Malý: *Light-Induced Precession of Magnetization in Ferromagnetic Semiconductor (Ga,Mn)As.* Acta Phys. Polon. A **118**, 1065 (2010).

[80] E. Rozkotová, P. Němec, D. Sprinzl, P. Horodyská, F. Trojánek, P. Malý, V. Novák, K. Olejník, M. Cukr, T. Jungwirth: *Laser-Induced Precession of Magnetization in GaMnAs*. IEEE Trans. Magn. **44**, 2674 (2008).

[81] H. Takechi, A. Oiwa, K. Nomura, T. Kondo, H. Munekata: *Light-induced precession of ferromagnetically coupled Mn spins in ferromagnetic (Ga,Mn)As.* Phys. Stat. Sol. (c) **3**, 4267 (2006).

[82] N. Tesařová, E. Rozkotová, H. Reichlová, P. Malý, V. Novák, M. Cukr,T. Jungwirth, P. Němec*: Influence of Magnetic Anisotropy on Laser-Induced Precession of Magnetization in Ferromagnetic Semiconductor (Ga, Mn)As*. J. Nanosc. Nanotechnol. **12**, 7477 (2012).

[83] Shah J.: *Ultrafast spectroscopy of semiconductors and semiconductor nanostructures*. Springer-Verlag, Berlin, Heidelberg, New York, 1996.

[84] J. Fernandez-Rossier, A. S. Nunez, M. Abolfath, and A. H. MacDonald: *Optical spin transfer torque in ferromagnetic semiconductors.* http://arxiv.org/abs/cond-mat/0304492.

[85] D. Fang, H. Kurebayashi, J. Wunderlich, K. Výborný, L. P. Zarbo, R. P. Campion, A. Casiraghi, B. L. Gallagher, T. Jungwirth, A. J. Ferguson: *Spin-orbit driven ferromagnetic resonance: A nanoscale magnetic characterisation technique*. Nat. Nanotechnol. **6**, 413 (2011).

[86] Kh. Khazen, H. J. von Bardeleben, M. Cubukcu, J. L. Cantin, V. Novak, K. Olejnik, M. Cukr, L. Thevenard, A. Lemaître: *Anisotropic magnetization relaxation in ferromagnetic* $Ga_{1-x}Mn_xAs$ *thin films*. Phys. Rev. B **78**, 195210 (2008).

[87] J. Sinova, T. Jungwirth, X. Liu, Y. Sasaki, J. K. Furdyna, W. A. Atkinson, A. H. MacDonald: *Magnetization relaxation in (Ga,Mn)As ferromagnetic semiconductors*. Phys. Rev. B **69**, 085209 (2004).

[88] J. Walowski, M. Djordjevic Kaufmann, B. Lenk, C. Hamann, J. McCord, M. Munzenberg: *Intrinsic and non-local Gilbert damping in polycrystalline nickel studied by Ti : sapphire laser fs spectroscopy*. J. Phys. D: Appl. Phys. **41**, 164016 (2008).

[89] A. A. Rzhevsky, B. B. Krichevtsov, D. E. Bürgler, C. M. Schneider: *Magnetization dynamics induced by ultrashort optical pulses in Fe/Cr thin films.* Phys. Rev. B **75**, 224434 (2007).

[90] X. Liu, Y. Y. Zhou, J. K. Furdyna: *Angular dependence of spin-wave resonances and surface spin pinning in ferromagnetic (Ga,Mn)As films*. Phys. Rev. B **75**, 195220 (2007).

[91] C. Bihler, W. Schloch, W. Limmer, S. T. B. Goennenwein, M. S. Brandt: *Spin-wave resonances and surface spin pinning in $Ga_{1-x}Mn_xAs$ thin films*. Phys. Rev. B **79**, 045205 (2009).

[92] D.M. Wang, Y.H. Rena, X. Liu, J.K. Furdyna, M. Grimsditch, R. Merlin: *Ultrafast optical study of magnons in the ferromagnetic semiconductor GaMnAs*. Superlatt. Microstruct. **41**, 372 (2007).

[93] E. Rozkotová: *Dynamika spinově polarizovaných nosičů náboje v polovodičích*. Diplomová práce, Univerzita Karlova v Praze, MFF, Praha (2007).

LIST OF ABBREVIATIONS

DMS	diluted magnetic semiconductor
EA	easy axis
FM	ferromagnetic
FMR	ferromagnetic resonance
IB	impurity band
MA	magnetocrystalline anisotropy
MBE	molecular beam epitaxy
MCD	magnetic circular dichroism
MLD	magnetic linear dichroism
MO	magneto-optical
OSTT	optical spin transfer torque
OSOT	optical spin-orbit torque
PKE	polar Kerr effect
SOC	spin-orbit coupling
SQUID	superconducting quantum interference device
SWR	spin wave resonance
TMR	tunneling magnetoresistance
VB	valance band

LIST OF IMPORTANT SYMBOLS

α	Gilbert damping constant
E_F	Fermi energy
F	free energy functional
g	Lande g-factor
γ	gyromagnetic ratio
H_{ext}	external magnetic field
K_c	cubic anisotropy
K_u	uniaxial anisotropy
K_{out}	out-of-plane anisotropy
μ_B	Bohr magneton
p	hole concentration
T_C	Curie temperature
T	temperature

APPENDICES

Contribution of Naďa Tesařová to attached articles

The results presented in this thesis are a part of an extensive research focused on the ferromagnetic semiconductors, where the (Ga,Mn)As is of the main interest. This research is done in a close collaboration with colleagues from the groups of Tomáš Jungwirth (Institute of Physics, Academy of Sciences in Prague), Václav Holý (Charles University in Prague), Brian Gallagher (University of Nottingham) and John Černe (University at Buffalo). Such a broad collaboration enables a very thorough investigation of the material properties by different experimental techniques, supported by a great theoretical background. This strongly focused research led to a publication of many articles where I am a co-author. However, in this theses I present only those papers where my contribution was major. More specifically, my contribution to the articles, which are presented in the Appendices below, is the following:

Appendix 1: T. Jungwirth, P. Horodyská, N. Tesařová, P. Němec, J. Šubrt, P. Malý, P. Kužel, C. Kadlec, J. Mašek, I. Němec, M. Orlita, V. Novák,1 K. Olejník, Z. Šrobáň , P. Vašek, P. Svoboda, J. Sinova: *Systematic Study of Mn-Doping Trends in Optical Properties of (Ga,Mn)As*. Phys. Rev. Lett. **105**, 227201 (2010).
I constructed the experimental set-up for the static MO measurements and measured all the MO data shown in the paper. I also contributed to the data analysis and to the manuscript writing.

Appendix 2: N. Tesařová, J. Šubrt, P. Malý, P. Němec, C. T. Ellis, A. Mukherjee, J. Cerne: *High Precision Magnetic Linear Dichroism Measurements in (Ga,Mn)As*. Accepted in Review of Scientific Instruments, arXiv:1212.0956.
I constructed the experimental set-up for the static MO measurements both in Prague and in Buffalo and I did all the experiments that are described in the paper. I performed the majority of the data analysis and of the manuscript writing.

Appendix 3: N. Tesařová, P. Němec, E. Rozkotová, F. Trojánek, P. Malý: *Light-Induced Precession of Magnetization in Ferromagnetic Semiconductor (Ga,Mn)As*. Acta Phys. Polon. A **118**, 1065 (2010).
I contributed to the construction of the experimental set-up for the time-resolved MO measurements. I measured all the data, performed their analysis, and wrote the article.

Appendix 4: N. Tesařová, E. Rozkotová, H. Reichlová, P. Malý, V. Novák, M. Cukr,T. Jungwirth, P. Němec: *Influence of Magnetic Anisotropy on Laser-Induced Precession of Magnetization in Ferromagnetic Semiconductor (Ga, Mn)As*. J. Nanosc. Nanotechnol. **12**, 7477 (2012).
I contributed to the construction of the experimental set-up for the time-resolved MO measurements. I measured all the MO data, performed their analysis, and wrote the article.

Appendix 5: N. Tesařová, P. Němec, E. Rozkotová, J. Šubrt, H. Reichlová, D. Butkovičová, F. Trojánek, P. Malý, V. Novák, T. Jungwirth: *Direct measurement of the three-dimensional*

magnetization vector trajectory in GaMnAs by a magneto-optical pump-and-probe method. Appl. Phys. Lett. **100**, 102403 (2012).
I contributed to the construction of the experimental set-up for the time-resolved MO measurements. I measured all the MO data, performed the data analysis and contributed to the analytical derivation of equations that describe the MO response of (Ga,Mn)As, which form the basis of this method for a determination of the real-space magnetization trajectory. I also contributed to the manuscript writing.

Appendix 6: P. Němec, E. Rozkotová, N. Tesařová, F. Trojánek, E. De Ranieri, K. Olejník, J. Zemen, V. Novák, M. Cukr, P. Malý, T. Jungwirth: *Experimental observation of the optical spin transfer torque*. Nat. Phys. **8**, 411 (2012).
I contributed to the construction of the experimental set-up for the time-resolved MO measurements but the time-resolved MO data reported in the main article were measured by Eva Rozkotová. I measured the majority of the experimental data that are shown in the Supplementary material to illustrate the universality of OSTT (Fig. 2 and Fig. 3a in the main article), the magnetic origin of the measured MO signals (Fig. 5 and Fig. 12 in the Supplementary material), and the probe-polarization sensitive measurements (Fig. 9a, Fig. 10, Fig. 11, and Fig. 13 in the Supplementary material). I also contributed to writing of both the main paper and the Supplementary material.

Appendix 7: N. Tesařová, P. Němec, E. Rozkotová, J. Zemen, T. Janda, D. Butkovičová, F. Trojánek, K. Olejník, V. Novák, P. Malý, T. Jungwirth: *Experimental observation of the optical spin-orbit torque*. Submitted to Nature Photonics, arXiv:1207.0307.
I contributed to the construction of the experimental set-up for the time-resolved MO measurements. I measured the MO data shown in Fig. 1, Fig. 2, and Fig. 3, performed their analysis, and contributed to the manuscript writing.
Note: Enclosed is the latest version of the manuscript that is currently in the 2nd round of the referee process in the Nature Photonics. This version is partially different from the version that is located at arXiv:1207.0307. The reason is that due to the Copyright policy of the Nature Publishing Group the revised version of the manuscript cannot be placed at arXiv before it is officially published in the corresponding journal.

Appendix 8: P. Němec, V. Novák, N. Tesařová, E. Rozkotová, H. Reichlová, D. Butkovičová, F. Trojánek, K. Olejník, P. Malý, R. P. Campion, B. I. Gallagher, J. Sinova, T. Jungwirth: *Establishing micromagnetic parameters of ferromagnetic semiconductor (Ga,Mn)As*. Accepted in Nature Communications, arXiv:1207.0310.
I contributed to the construction of the experimental set-up for the time-resolved MO measurements. I measured the MO data and performed the numerical data modeling that are shown in Fig. 1b, c, in Fig. 4 and in Fig. 5. I also contributed to the manuscript writing.
Note: Enclosed is the latest version of the manuscript that was accepted in the Nature Communications. This version is partially different from the version that is located at arXiv: 1207.0310. The reason is that due to the Copyright policy of the Nature Publishing Group the revised version of the manuscript cannot be placed at arXiv before it is officially published in the corresponding journal.

APPENDIX 1

Authors: T. Jungwirth, P. Horodyská, N. Tesařová, P. Němec, J. Šubrt, P. Malý, P. Kužel, C. Kadlec, J. Mašek, I. Němec, M. Orlita, V. Novák,1 K. Olejník, Z. Šrobáň , P. Vašek, P. Svoboda and J. Sinova

Title: Systematic Study of Mn-Doping Trends in Optical Properties of (Ga,Mn)As

Journal: Physical Review Letters

Volume: 105

Article Number: 227201

Year: 2010

APPENDIX 2

Authors: N. Tesařová, J. Šubrt, P. Malý, P. Němec, C. T. Ellis, A. Mukherjee and J. Cerne

Title: High Precision Magnetic Linear Dichroism Measurements in (Ga,Mn)As

Journal: accepted in Review of Scientific Instruments

Preprint server: http://arxiv.org/abs/1212.0956

APPENDIX 3

Authors: N. Tesařová, P. Němec, E. Rozkotová, F. Trojánek and P. Malý

Title: Light-Induced Precession of Magnetization in Ferromagnetic Semiconductor (Ga,Mn)As

Journal: Acta Physica Polonica A

Volume: 118

Article Number: 1065

Year: 2010

APPENDIX 4

Authors: N. Tesařová, E. Rozkotová, H. Reichlová, P. Malý, V. Novák, M. Cukr,T. Jungwirth and P. Němec

Title: Influence of Magnetic Anisotropy on Laser-Induced Precession of Magnetization in Ferromagnetic Semiconductor (Ga, Mn)As

Journal: Journal of Nanoscience and Nanotechnology

Volume: 12

Article Number: 7477

Year: 2012

APPENDIX 5

Authors: N. Tesařová, P. Němec, E. Rozkotová, J. Šubrt, H. Reichlová, D. Butkovičová, F. Trojánek, P. Malý, V. Novák and T. Jungwirth

Title: Direct measurement of the three-dimensional magnetization vector trajectory in GaMnAs by a magneto-optical pump-and-probe method

Journal: Applied Physical Letters

Volume: 100

Article Number: 102403

Year: 2012

APPENDIX 6

Authors: P. Němec, E. Rozkotová, N. Tesařová, F. Trojánek, E. De Ranieri, K. Olejník, J. Zemen, V. Novák, M. Cukr, P. Malý and T. Jungwirth

Title: Experimental observation of the optical spin transfer torque

Journal: Nature Physics

Volume: 8

Article Number: 411

Year: 2012

APPENDIX 7

Authors: N. Tesařová, P. Němec, E. Rozkotová, J. Zemen, T. Janda, D. Butkovičová, F. Trojánek, K. Olejník, V. Novák, P. Malý and T. Jungwirth

Title: Experimental observation of the optical spin-orbit torque

Journal: submitted to Nature Photonics

Preprint server: http://arxiv.org/abs/1207.0307

APPENDIX 8

Authors: P. Němec, V. Novák, N. Tesařová, E. Rozkotová, H. Reichlová, D. Butkovičová, F. Trojánek, K. Olejník, P. Malý, R. P. Campion, B. I. Gallagher, J. Sinova and T. Jungwirth

Title: Establishing micromagnetic parameters of ferromagnetic semiconductor (Ga,Mn)As

Journal: accepted in Nature Communications

Preprint server: http://arxiv.org/abs/1207.0310

APPENDIX 9

Experimental setup for the time-resolved MO spectroscopy measurements

All the time-resolved measurements presented in this thesis were done in the experimental setup described in Fig. A9.1. The titan-sapphire laser was used to generate ultrashort laser pulses (width of the pulse ~ 200 fs) with a repetition rate of 82 MHz. The laser system can be tuned in the spectral range of 720 – 1050 nm, but we typically used the wavelength λ = 760 nm (phonon energy hv = 1.63 eV) which is sufficient to excite (Ga,Mn)As above the band gap. The laser pulses were divided by the beam splitter into two parts – the stronger pump pulse and the weaker probe pulse. The pump pulse was time-delayed by a computer-controlled delay line with respect to the probe pulse. The intensity of the laser pulses was individually adjusted in both arms by the neutral density filters. The polarization state was controlled by the polarizers and the wave plates (half and quarter wave plates), where the pump pulses were typically circularly polarized and the probe pulses were polarized linearly. The laser beams were focused on the sample in a near normal incidence geometry (the angles of incidence, measured from the normal of the sample, for pump and probe beams were 3º and 9º, respectively). The samples were glued on the cold finger (by a silver paste which enabled a good thermal conductivity) of a closed-cycle cryostat. The samples were typically cooled down to 15 K. The samples were placed between the poles of the electromagnet, which could generate a magnetic field (H_{ext}) up to ~ 600 mT.

After reflection from the sample, the probe pulses were analyzed in the optical bridge (while the reflected pump beam was blocked). The basic principle of the optical bridge is, that the linear polarization of the probe beam is divided by a polarizing beam splitter into *s*- and *p*-orthogonal polarizations (usually a half wave plate is placed in front of the beam splitter that can be used to adjust an equal intensities of the *s*- and *p*- polarized beams). Each of the polarizations is deflected into different arms of the optical bridge where they are separately detected by photodiodes. The output signals from the photodiods are transferred to differential preamplifiers where the sum and the difference from the individual signals are computed. These differential and sum signals are further amplified and both are processed by the lock-in amplifiers, that were synchronized to the reference signal from the optical chopper. The chopper was placed in the pump beam, so the detected signal reflects only the magneto-optical signal changes induced by the pump pulses.

The sum signal provides information about the pump-induced reflectivity change of the sample $\Delta R(t)$ that can by expressed as [93]:

$$\frac{\Delta R(t)}{R_0} \approx \frac{\Delta I_p(t)+\Delta I_s(t)}{I_0^p+I_0^s}, \qquad \text{(A1)}$$

where R_0 is the static reflectivity of the sample, ΔI_p (ΔI_s) is the pump-induced change of the intensity in the *p*- (*s*-) polarized arm of the optical bridge with respect to intensities without the pump pulse I_0^p (I_0^s).

The difference signal is related to the pump-induced rotation of the polarization plane $\Delta\theta$ (or to the pump-induced ellipticity, if a quarter wave plate is placed in front of the half wave plate in the optical bridge) that can be expressed as [93]:

$$\Delta\theta(t) = \frac{\Delta I_p(t) - \Delta I_s(t)}{2(I_0^p + I_0^s)}. \qquad \text{(A2)}$$

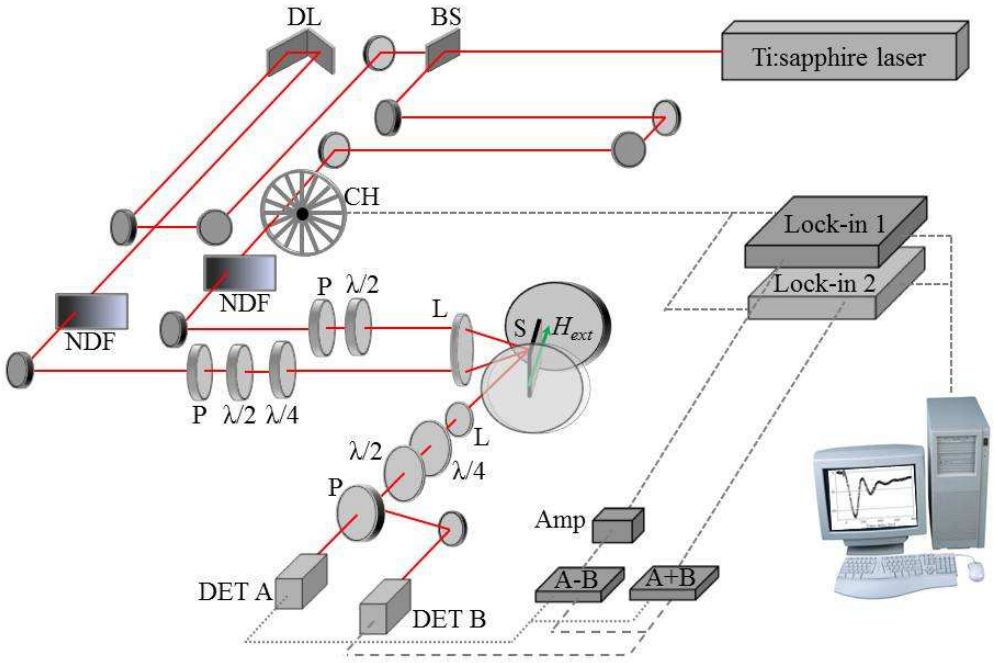

Fig. A9.1: Experimental setup for the time-resolved MO measurements. The meaning of the abbreviations is the following: BS – beam splitter, DL – delay line, CH – chopper, NDF – neutral density filter, P – polarizer, λ/2 – half wave plate, λ/4 – quarter wave plate, L – lens, S – sample, H_{ext} – external magnetic field generated between the poles of the electromagnet, DET A (B) – silicon detectors, A-B, A+B – differential preamplifiers, AMP – preamplifier, lock-in 1 (2) – phase sensitive lock-in amplifier.